J. Fluid Mech. (2010), *vol.* 662, *pp.* 134–172.
doi:10.1017/S0022112010003162

The diffusive strip method for scalar mixing in two dimensions

P. MEUNIER[1]† AND E. VILLERMAUX[1,2]

[1]Institut de Recherche sur les Phénomènes Hors Equilibre (IRPHE), CNRS, Aix-Marseille Université, 13384 Marseille Cedex 13, France

[2]Institut Universitaire de France, 75005 Paris, France

(Received 18 December 2009; revised 7 June 2010; accepted 7 June 2010; first published online 6 September 2010)

We introduce a new numerical method for the study of scalar mixing in two-dimensional advection fields. The position of an advected material strip is computed kinematically, and the associated convection–diffusion problem is solved using the computed local stretching rate along the strip, assuming that the diffusing strip thickness is smaller than its local radius of curvature. This widely legitimate assumption reduces the numerical problem to the computation of a single variable along the strip, thus making the method extremely fast and applicable to any large Péclet number. The method is then used to document the mixing properties of a chaotic sine flow, for which we relate the global quantities (spectra, concentration probability distribution functions (PDFs), increments) to the distributed stretching of the strip convoluted by the flow, possibly overlapping with itself. The numerical results indicate that the PDF of the strip elongation is log normal, a signature of random multiplicative processes. This property leads to exact analytical predictions for the spectrum of the field and for the PDF of the scalar concentration of a solitary strip. The present simulations offer a unique way of discovering the interaction rule for building complex mixtures which are made of a random superposition of overlapping strips leading to concentration PDFs stable by self-convolution.

Key words: chaotic advection, turbulent mixing

1. Introduction

Fluid mechanics has for a long time relied on observations, experiments and data collection rationalized by first principles theories or *ad hoc* models and correlations. The output was a corpus of formulas, abacus and charts made available to the engineer, meteorologist, physicist, etc for helping him to solve practical problems. Originally motivated by weather-forecasting issues, and since the basic equations describing fluids were known, the idea of re-creating natural phenomena by artificial means using automatic calculations arose, probably first formalized in this form by Lewis Fry Richardson (Richardson 1922). Since then, the numerical simulation of fluid flows has undergone a dramatic growth, and the methods are continuously improving to make the computations faster and more faithful to reality.

† Email address for correspondence: meunier@irphe.univ-mrs.fr

For scalar mixing, namely the homogenization of a dye, or impurity in a prescribed flow field, the existing methods can be roughly grouped into two main categories:

(i) Lagrangian methods follow the position $\boldsymbol{x}_i$ of passive tracers in the flow by integrating the equation of motion

$$\frac{\mathrm{d}\boldsymbol{x}_i}{\mathrm{d}t} = \boldsymbol{v}(\boldsymbol{x}_i, t), \tag{1.1}$$

in a velocity field $\boldsymbol{v}(\boldsymbol{x}_i, t)$ given *a priori*. This method is useful to study trajectories, the flow kinematics and stirring properties; it is widely used in the context of chaos, maps and ergodic theory (e.g. Jones 1994; Phelps & Tucker 2006; Sturman, Ottino & Wiggins 2006; Robinson, Cleary & Monaghan 2008). It does not, however, incorporate explicitly diffusion effects, those which are nevertheless ultimately responsible for mixing.

(ii) Eulerian methods on the other hand deal with the markers concentration field c (the number density of the markers coarse-grained on a grid) by solving a partial differential equation, namely the diffusion–advection equation

$$\frac{\partial c}{\partial t} + \boldsymbol{v} \cdot \nabla c = D\Delta c, \tag{1.2}$$

where D is the tracers diffusivity and Δ is the Laplacian operator. The method provides the whole concentration field accounting explicitly for diffusion, but needs a discretization grid of space to compute gradients, and remains, therefore, limited to smooth concentration fields with not too sharp gradients for reasonable computation times and cost (Sukhatme & Pierrehumbert 2002; Fereday & Haynes 2004; Perugini *et al.* 2004; Shankar & Kidambi 2009).

Many other specific methods exist, particularly for turbulent flows, with possibly an admixture of models to represent small unsolved subgrid scales, and/or additional effects such as buoyancy, chemical reactions, heat release, etc. (see e.g. Yeung 2002; Fox 2004).

The diffusive strip method we introduce here is an extension of ideas developed to handle scalar diffusion on a moving substrate. The method amounts to reducing the full convection–diffusion problem in (1.2) to a simpler, analytically tractable diffusion equation in suitably chosen coordinates as

$$\frac{\partial c}{\partial \tau} = \frac{\partial^2 c}{\partial \tilde{n}^2}, \tag{1.3}$$

where τ and $\tilde{n}$ are functions of space, time, scalar diffusivity and of the structure of the velocity field, respectively. The method for going from (1.2) to (1.3) and finding closed form, nearly exact solutions has been used in the context of heat transfer (Levèque 1928), turbulence (Batchelor 1959; Villermaux & Duplat 2003), combustion (Marble & Broadwell 1977; Marble 1988), engineering and process industry (Mohr, Saxton & Jepson 1957; Ranz 1979; Villermaux & Rehab 2000; Meunier & Villermaux 2003), geophysics (Rhines & Young 1983; Allègre & Turcotte 1986), chaos (Ottino 1989; Beigie, Leonard & Wiggins 1991), physics (Moffatt 1983; Meunier & Villermaux 2007) or mathematics (Fannjiang, Nonnenmacher & Wolonski 2004).

In these works, the method has been successfully used for computing mixing times and length scales. However, the method can potentially provide more since it gives access to the evolution of the whole concentration field, with a direct, nearly exact link with the initial Fourier equation (1.2). For instance, in the simple case of a strip wrapping around a vortex (Meunier & Villermaux 2003, 2007), the position

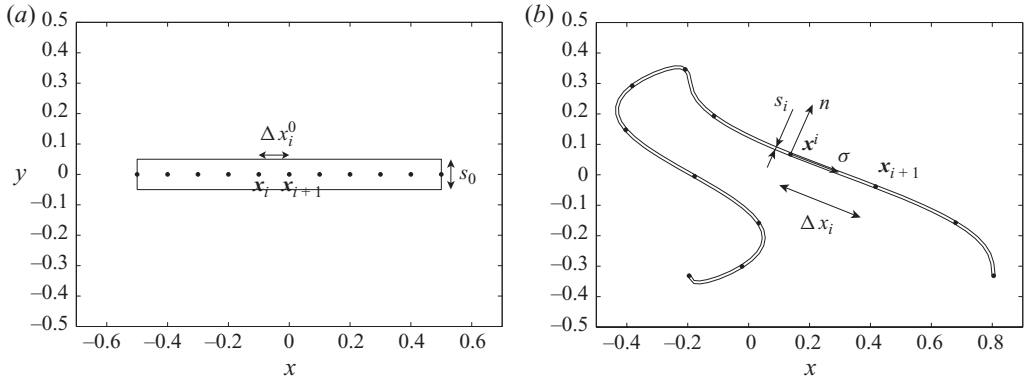

FIGURE 1. Schematic drawing of the evolution of a strip defined by the points $\boldsymbol{x}_i$ and a striation thickness s_i initially equal to s_0.

and the stretching rate of the strip are known explicitly from the velocity field in a straightforward manner, which allows derivation of the whole concentration field analytically, at any time. Building on this elementary step, we generalize here the method to *a priori* any velocity field however complicated it may be. We first present the method, its numerical implementation and validation in § 2, and then apply it to study the mixing properties (internal structure, interaction rule, concentration distribution, spectra, increments, kinetics) of a prototype flow, namely the sine flow in §§ 3–7. The details of the numerics and the computational cost of the method are discussed in the Appendix.

2. The diffusive strip: a new numerical method

2.1. *The method*

The flow field $\boldsymbol{v}(\boldsymbol{x}, t)$ is assumed to be given analytically, decoupled from the concentration field itself (passive scalar), but not necessarily integrable. It is incompressible and two-dimensional. A scalar strip is described by the position of tracers located in $\boldsymbol{x}_i$, which are advected by solving numerically the equation of motion (1.1). The tracers are initially separated by a length Δx_i^0, as shown in figure 1. The problem is considered in an open domain, except in § 6.3 where the tracers are placed periodically in order to render the problem periodic. Then we suppose that the strip contains a scalar c, whose concentration has initially a Gaussian transverse profile with a striation thickness s_0,

$$c(n) = c_0 \, \mathrm{e}^{-n^2/s_0^2}, \quad \text{at } t = 0. \tag{2.1}$$

Here, n is the local coordinate normal to the strip (see figure 1). The particular choice of a Gaussian is not restrictive. It simply expresses that the strip is localized in space, and has a typical width s_0 initially. We wish to know how the transverse profile evolves when the strip is advected by the flow. The evolution equation for the scalar $c(\boldsymbol{x}, t)$ is the standard diffusion–advection equation (1.2).

In the absence of diffusion, the strip is stretched and thus experiences a contraction in the transverse direction due to incompressibility. Its striation thickness $s_i(t)$ decreases with time and can be calculated numerically by applying the conservation

of areas

$$s_i = \frac{s_0 \Delta x_i^0}{\Delta x_i}. \tag{2.2}$$

Here, $\Delta x_i = ||\boldsymbol{x}_{i+1} - \boldsymbol{x}_i||$ is the distance between two consecutive tracers. Around a tracer x_i, the velocity field in a local frame of reference (σ, n) aligned with the strip is given by

$$v_\sigma = -\frac{\sigma}{s_i}\frac{\mathrm{d}s_i}{\mathrm{d}t} + \frac{\partial v_\sigma}{\partial n} n, \tag{2.3}$$

$$v_n = \frac{n}{s_i}\frac{\mathrm{d}s_i}{\mathrm{d}t}. \tag{2.4}$$

It is a Taylor expansion at first order of the flow around $\boldsymbol{x}_i$. The velocity field at the position of the tracer $\boldsymbol{x}_i$ vanishes because the frame of reference is centred in $\boldsymbol{x}_i$. The velocity gradient $\partial v_\sigma/\partial\sigma$ is by definition equal to $\mathrm{d}\ln s_i/\mathrm{d}t$. The velocity gradient $\partial v_n/\partial\sigma$ vanishes because the frame of reference is aligned with the strip at any time. The velocity gradient $\partial v_n/\partial n$ is equal to $-\mathrm{d}\ln s_i/\mathrm{d}t$ due to incompressibility. The velocity gradient $\partial v_\sigma/\partial n$ is unknown. However, as time evolves, the length scale in the transverse direction gets much smaller than the length scale along the strip. The transverse scalar gradient $\partial c/\partial n$ is thus much larger than the scalar gradient along the strip $\partial c/\partial\sigma$. We can thus neglect the term $v_\sigma \partial c/\partial\sigma$ in front of the term $v_n \partial c/\partial n$ in the advection term of (1.2) (Dimotakis & Catrakis 1999). The same reasoning holds for the diffusion term such that the advection–diffusion equation (1.2) close to $\boldsymbol{x}_i$ becomes

$$\frac{\partial c}{\partial t} + \frac{n}{s_i}\frac{\mathrm{d}s_i}{\mathrm{d}t}\frac{\partial c}{\partial n} = D\frac{\partial^2 c}{\partial n^2}. \tag{2.5}$$

The exact partial differential equation would contain two additional terms corresponding to $v_\sigma \partial c/\partial\sigma$ on the left-hand side and an additional term $D\partial^2 c/\partial\sigma^2$ on the right-hand side. This asymptotic partial differential equation has already been used in this form in the works mentioned in § 1. The impact of the flow is all concentrated in the rate of change of the striation thickness $\mathrm{d}\ln s_i/\mathrm{d}t$. This equation holds in flows which tend to form elongated structures (strips in two dimensions), as it is the case for most flows in nature, may they be random, or deterministic (see the early drawings of Welander (1955), and more recent observations, including in three dimensions, where the flow forms *sheets* as in Buch Jr. & Dahm 1996; Fountain, Khakhar & Ottino 1998). It does not describe, however, regions of folded strips whose radius of curvature is of the order of their thickness. We will come back to this point in § 2.5. Equation (2.5) can be simplified by using a change of variable (Ranz 1979) where the transverse distance n is non-dimensionalized by the striation thickness $\tilde{n} = n/s_i(t)$, and the time is counted in units of the current diffusion time $s_i(t)^2/D$ as

$$\frac{\mathrm{d}\tau_i}{\mathrm{d}t} = \frac{D}{s_i(t)^2}. \tag{2.6}$$

The dimensionless time τ_i for the tracer $\boldsymbol{x}_i$ can be easily calculated numerically during the integration of the equation of motion (1.1) since the striation thickness s_i is known through (2.2). Using these new variables, the equation for the scalar c becomes a simple diffusion equation

$$\frac{\partial c}{\partial \tau} = \frac{\partial^2 c}{\partial \tilde{n}^2}. \tag{2.7}$$

The initial condition at $\tau = 0$ (corresponding to $t = 0$) is $c(\tilde{n}) = c_0 \exp(-\tilde{n}^2)$. The solution is a Gaussian profile at any time, which can be rewritten as a function of the dimensional coordinate n as

$$c(n,t) = \frac{c_0}{\sqrt{1+4\tau_i(t)}} \exp\left(-\frac{n^2/s_i(t)^2}{1+4\tau_i(t)}\right). \tag{2.8}$$

Leonard (2009) has shown that the same reasoning can be done without neglecting the gradients along the strip ($\partial/\partial\sigma$) if the coordinate σ is dimensionalized by $1/s_i(t)$. This divides the normal profile (2.7) by a factor $\sqrt{1+4\hat{\tau}}$ which tends to 1 for large Péclet numbers, because $\hat{\tau}(t) = D\int s_i(t')^2\,\mathrm{d}t'$ tends to 0 for vanishing D (since s_i decreases exponentially in time, making the integral convergent).

It is thus sufficient to compute numerically the position of the tracers $\boldsymbol{x}_i$, the striation thickness s_i and the dimensionless time τ_i as a function of time by integrating equations (1.1), (2.2) and (2.6) to know the transverse profile of the scalar $c(n,t)$ across the strip, and thus to have access to the spatial distribution of the scalar initially contained in the strip. We will see in § 2.4 how to reconstruct numerically the scalar field $c(\boldsymbol{x},t)$ knowing these quantities.

The dimensionless time τ is proportional to the diffusivity D. It is thus sufficient to make a single numerical calculation with $D = 1$ to get the result for any diffusivity by multiplying τ_i by the desired value D at the end of the computation. The initial striation thickness s_0 can also be changed easily *a posteriori* since the striation thickness s_i is proportional to s_0 and the dimensionless time is proportional to s_0^{-2}.

2.2. *An example*

Let us take the simple example of a strip of initial thickness s_0 and length L_0, uniformly stretched at a rate γ. Its current length is $L(t) = L_0\mathrm{e}^{\gamma t}$ while its striation thickness decreases as $s_0\mathrm{e}^{-\gamma t}$. According to (2.8), the maximal concentration in the strip (in $\tilde{n} = 0$) will start to decay when $\tau(t)$ becomes of order unity. From (2.6), one has

$$\tau(t) = \frac{D}{2\gamma s_0^2}\left(\mathrm{e}^{2\gamma t} - 1\right), \tag{2.9}$$

and the condition $\tau(t_s) = O(1)$ defines the mixing time t_s depending on a Péclet number Pe as

$$t_s = \frac{1}{2\gamma}\ln Pe, \quad \text{with} \quad Pe = \frac{\gamma s_0^2}{D}. \tag{2.10}$$

From this critical time, it is seen from (2.8) that the maximal concentration in the strip decays exponentially as

$$c(0,t) \sim \mathrm{e}^{-\gamma(t-t_s)}, \tag{2.11}$$

and that the strip transverse size remains constant and equal to

$$s(t_s) = \sqrt{\frac{D}{\gamma}} = s_0\, Pe^{-1/2}, \tag{2.12}$$

the length scale equilibrating substrate compression and diffusion broadening. It is called the Batchelor scale (Batchelor 1959).

2.3. *Strip refinement*

The strip diffusion method is based on the property that the strip will be stretched by the flow and thus becomes ever thinner and elongated. The main advantage is

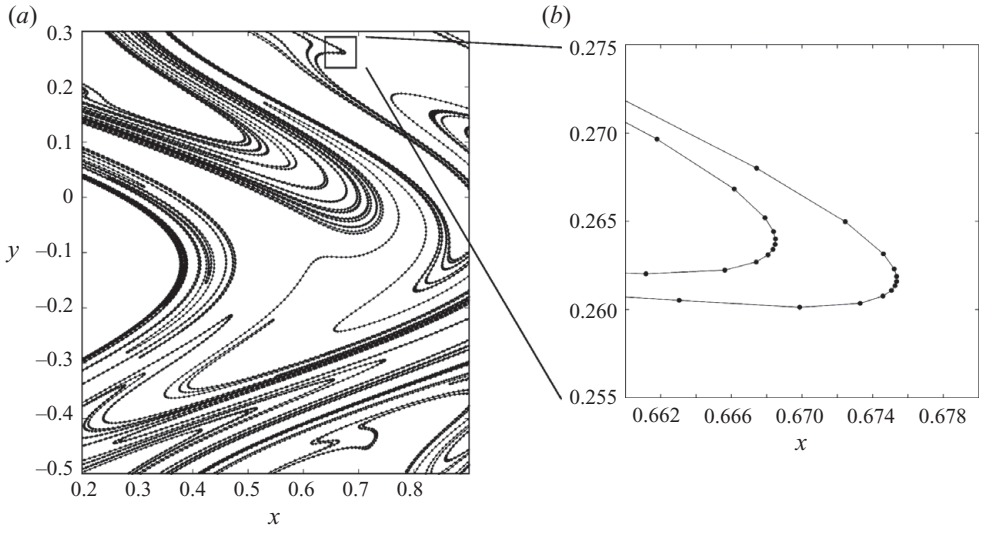

FIGURE 2. Example of the position of the strip in a disordered flow (sine flow), showing the appearance of cusps along the strip. A zoom of a cusp shows that the distribution of points along the strips is denser at the cusp, i.e. when the curvature increases. The numerical constants defined by (2.13) are $\Delta l = 0.01$ and $\alpha = 10\Delta l/\pi$.

that it allows to neglect diffusion along the strip since concentration gradients in that direction essentially vanish. However, a direct consequence is that the distance between two consecutive tracers increases with time. We will see below that the total length of the strip increases linearly in time for the case of a vortex (§ 2.6) and exponentially in time for the sine flow (§ 3). It is thus necessary to refine the strip such that it is always well represented geometrically, as was noted by Cerbelli, Alvarez & Muzzio (2002). This refinement was implemented every 10 time steps, and was thus very weakly time consuming.

The first idea would be to increase the number of points at each refinement such that the distance between two tracers $||\boldsymbol{x}_{i+1} - \boldsymbol{x}_i||$ is equal to a constant, say Δl. However, disordered flows bend the strip and create cusps with a very high curvature, as can be seen in figure 2 for the sine flow. The refinement must then be denser in the regions with high curvatures. A good criterion is to refine the strip such that the distance between two consecutive points is equal to

$$||\boldsymbol{x}_{i+1} - \boldsymbol{x}_i|| = \frac{\Delta l}{1 + \alpha\kappa}, \tag{2.13}$$

where κ is the curvature of the strip and Δl and α are numerical constants. Δl corresponds to the distance between two tracers in the regions with low curvature. α governs the number of tracers in the regions with high curvature: the algorithm adds a number of points equal to $\pi\alpha/\Delta l$ if the cusps makes a 180° turn. This refinement is illustrated in figure 2, where the distance between two consecutive points is much smaller at the cusp than in the other regions with low curvatures. The numerical method to do so is presented in the Appendix.

This refinement has proven to be very efficient, even in the case of the sine flow, which stretches the strip exponentially in time and has thus a strong sensitivity to initial conditions. The main disadvantage is that the size of the variables $(\boldsymbol{x}_i, s_i, \tau_i)$ increases with time and that the algorithm thus gets slower and slower at late stages,

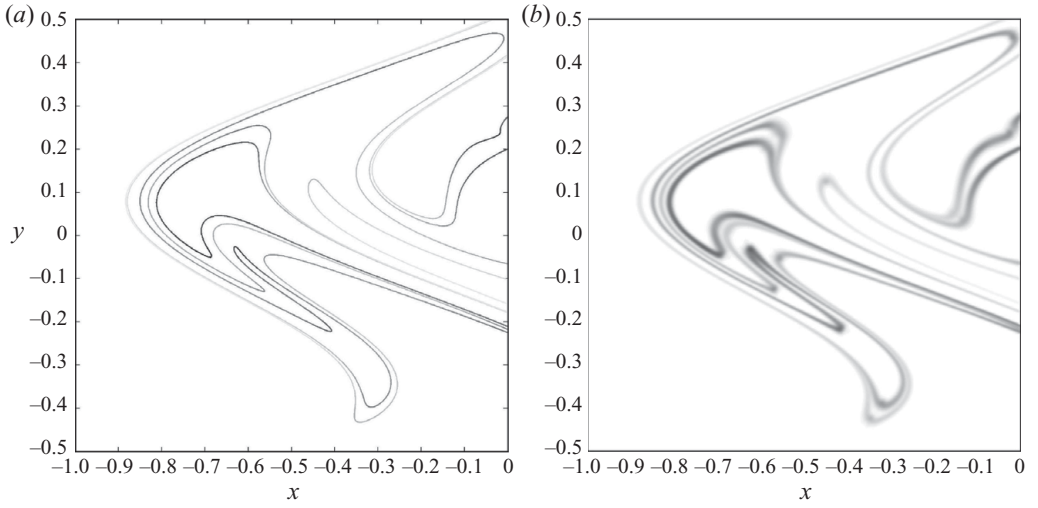

FIGURE 3. Examples of the distribution of scalar obtained by plotting a line (a) and by reconstructing the scalar on a grid using (2.14) (b). The distance Δl between two tracers during the reconstruction is equal to 0.0065 and the mesh size is equal to 0.001. The flow is a sine flow at $t = 4$ and $Pe = 10^5$ and initial thickness of the strip is $s_0 = 0.05$.

although the algorithm is extremely fast to compute the early stages. However, we will see in the following that it is sufficient to reach the mixing time even for Péclet number up to 10^{10}. This allows the obtaining of very interesting properties of the diffusion process at these Péclet numbers, which would otherwise be impossible using standard algorithms.

2.4. *Reconstruction of the scalar field*

We have shown in § 2.1 how to calculate numerically the transverse profile $c(n)$ of a strip of scalar given by (2.8) by integrating a simple equation (2.6) for the dimensionless times τ_i during the integration of the motion of the tracers $\boldsymbol{x}_i$. We wish to reconstruct the spatial distribution of scalar using this information. The easiest method is to draw a line, with a colour corresponding to the maximum of the transverse profile. This means that each segment $[\boldsymbol{x}_i\, \boldsymbol{x}_{i+1}]$ is plotted with a colour corresponding to $c_0/\sqrt{1+4\tau_i}$. An example plotted in figure 3(a) shows that it gives very good information on the position and concentration of the scalar. This method is extremely useful for large Péclet numbers, when the strip is so thin that its thickness get smaller than the resolution of the figure. Moreover, it is very fast and allows a field of scalar to be drawn almost instantaneously. However, this line drawing technique is not suitable as soon as several strips get so close to each other that their concentration profiles overlap.

We thus need to reconstruct the distribution of scalar on a two-dimensional grid. This task is much more tedious than the previous technique. It is very demanding in memory since the grid must be as narrow as possible, and it is also very unstable at the cusps, where the model fails. The correct treatment of the cusps is detailed in § 2.5.

The first step is to reinterpolate the strip such that the distance between two tracers is constant and equal to Δl. In the reconstruction process, Δl was chosen equal to the mean thickness of the strip which is easily calculated numerically as $\langle s_i\sqrt{1+4\tau_i}\rangle$, with s_i the striation thickness. Once the tracers are equally spaced, the distribution of

scalar can be reconstructed by adding small Gaussian ellipses centred on each tracer

$$c(\boldsymbol{x}) = \sum_i \frac{c_0/1.7726}{\sqrt{1+4\tau_i}} \exp\left\{ -\frac{[(\boldsymbol{x}-\boldsymbol{x}_i)\cdot\widehat{\boldsymbol{\sigma}}_i]^2}{\Delta l^2} - \frac{[(\boldsymbol{x}-\boldsymbol{x}_i)\cdot\widehat{\boldsymbol{n}}_i]^2}{s_i^2(1+4\tau_i)} \right\}. \tag{2.14}$$

Here, $\widehat{\boldsymbol{\sigma}}_i$ and $\widehat{\boldsymbol{n}}_i$ are the unit vectors tangent and normal, respectively, to the strip. The ellipses have a major axis oriented along the strip, with a parameter of the Gaussian profile equal to Δl. Their minor axis is normal to the strip with a parameter $s_i\sqrt{1+4\tau_i}$ as prescribed by the model. The constant 1.7726 is due to the overlap of the ellipses: since they are separated by Δl and have a Gaussian profile along the strip with a parameter Δl, the maximal concentration is overestimated by a factor $\sum_{j=-\infty}^{j=+\infty} \mathrm{e}^{-j^2} = 1.7726$. It can be noted that it is easier numerically to centre the ellipses around the middle point of $[\boldsymbol{x}_i\,\boldsymbol{x}_{i+1}]$ since the unit vectors $\widehat{\boldsymbol{\sigma}}_i$ and $\widehat{\boldsymbol{n}}_i$ are then easier to calculate.

An example of such a reconstruction is plotted in figure 3(*b*). The picture is similar to the one of figure 3(*a*). But here, the strip has a Gaussian transverse profile with the correct thickness. The overlap of the ellipses along the strip is not visible although they are separated by five times the mesh size. Different parts of the strip can mix together, for example at $\boldsymbol{x} = (-0.55, 0.15)$, which shows that the model is still valid in the case of strip overlap or aggregation (see § 6.3 for a precise definition of this notion).

The strip is well defined in the regions with low curvatures. Its thickness is usually small when its concentration is small. This is consistent with the diffusion process since it corresponds to high stretching rates. The model thus describes well the diffusion of the strip although its calculation was not implemented on a two-dimensional grid, but only modelled assuming that the strip is thin. This assumption fails when the radius of curvature gets of the order of the thickness of the strip, i.e. at the cusps. These regions are treated separately in § 3.

2.5. *Post-treatment of cusps*

In regions with high curvature, the model fails because the thickness becomes of the order of the radius of curvature. There, the diffusion problem is no longer essentially one-dimensional, contrary to the assumption leading to (2.5). This poses two numerical problems in the reconstruction of the distribution of scalar. The first one arises even in the absence of diffusion, and comes from the superposition of the strip from both sides of the cusp. As shown in figure 4(*a*), if the distance d between these two sides of the cusp is smaller than twice the thickness s_i of the strip, there will be some overlap of these two parts of the strip and the concentration c of the scalar can be two times higher than the initial concentration c_0, which is not physical. The best way to prevent these overlaps is to reduce the thickness of the strip by reducing the initial thickness s_0. In our simulation, an initial thickness $s_0 = 0.05$ would lead to only 0.1 % of the tracers where the distance d is smaller than twice s_i. For these points, the algorithm modifies the initial thickness only locally by decreasing s_i to $d/2$ and also changing the dimensionless time τ_i accordingly: it is multiplied by a factor $4s_i^2/d^2$ (since τ is proportional to s_0^{-2}). It is true that this procedure does not conserve the total quantity of scalar, but the loss was usually less than 0.1 %. This procedure does not modify at all the probability distribution functions (PDFs) of scalar or the spectra since these problems are localized in very small areas and do not contribute appreciably to the global quantities. This treatment is only necessary to prevent small dots of high concentration appearing in the spatial concentration distribution.

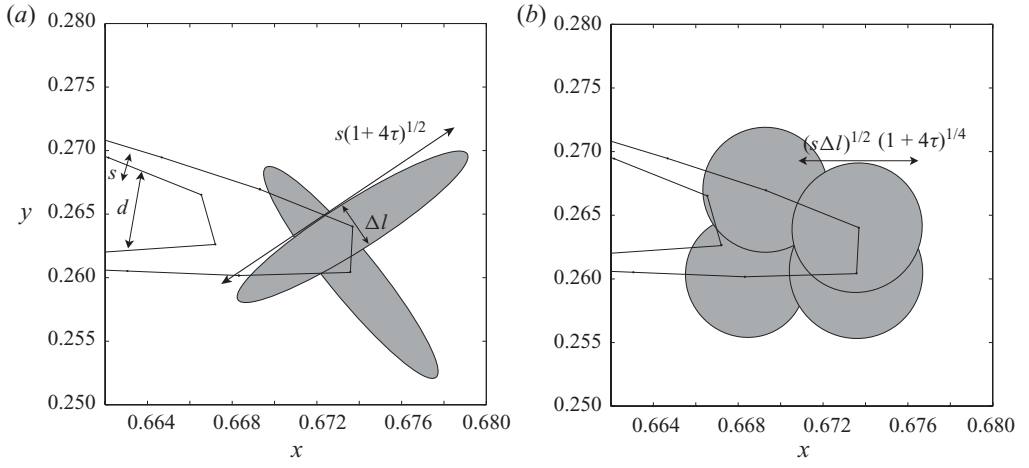

FIGURE 4. Regularization of the scalar field around a cusp during the reconstruction process.

A second problem arises in the presence of diffusion. Indeed, for rather large diffusivities ($Pe < 10^5$), we observed some lines of high concentration of scalar centred around the cusps. They are represented schematically in figure 4(a) by the two grey ellipses centred around the two tracers of the cusp. Such a numerical problem arises when the thickness of the strip, equal to $s_i\sqrt{1+4\tau_i}$, is larger than the distance Δl between two consecutive tracers. We observed this phenomenon at only a few points of the scalar field (usually less than 10 cusps in the simulation of the sine flow in § 3), but these ellipses would contaminate the whole field. We thus treated them by replacing the ellipses by circles with the same area, such that the total quantity of scalar is conserved. This procedure was very efficient in solving this numerical problem, although it is not a clean treatment of theses cusps. However, as was said previously, these problems arise in very small areas and do not contribute appreciably to the global quantities such as PDF and spectra. It is thus sufficient to use these basic procedures. To properly treat these cusps, it might be possible to modify the model such that the diffusion is calculated numerically on a two-dimensional mesh in the neighbourhood of the cusp.

2.6. *Validation: flow in a point vortex*

In this section, meant to validate our method, we present the results of the strip diffusion method for the case of a point vortex with circulation $\Gamma = 14.2$ cm^2 s^{-1} located in $\boldsymbol{x} = 0$, for which an experiment exists (Meunier & Villermaux 2003). The scalar is injected initially along the x-axis in order to mimic the experiment. The initial thickness $s_0 = 0.11$ cm is chosen two times smaller than the experimental one ($s_0 = 0.22$ cm) such that the final theoretical profiles are equal. Indeed, in the original study of Meunier & Villermaux (2003), s_0 is the width of a square profile, whereas here, s_0 is the parameter of a Gaussian profile. Initially, the scalar is injected along the x-axis between $x = 0.6$ cm and $x = 1.8$ cm.

Figure 5 shows the spatial distribution of scalar at $t = 10$ s for various diffusivities. As observed experimentally, the strip rolls up around the vortex centre and creates a spiral. For a very small diffusivity ($D = 10^{-8}$ cm^2 s^{-1}), the scalar has not yet reached the mixing time and the maximal concentration across the strip is equal to the initial concentration c_0 almost everywhere (figure 5a). For a slightly larger diffusivity ($D = 10^{-6}$ cm^2 s^{-1}), the scalar has started to diffuse and its maximal concentration has

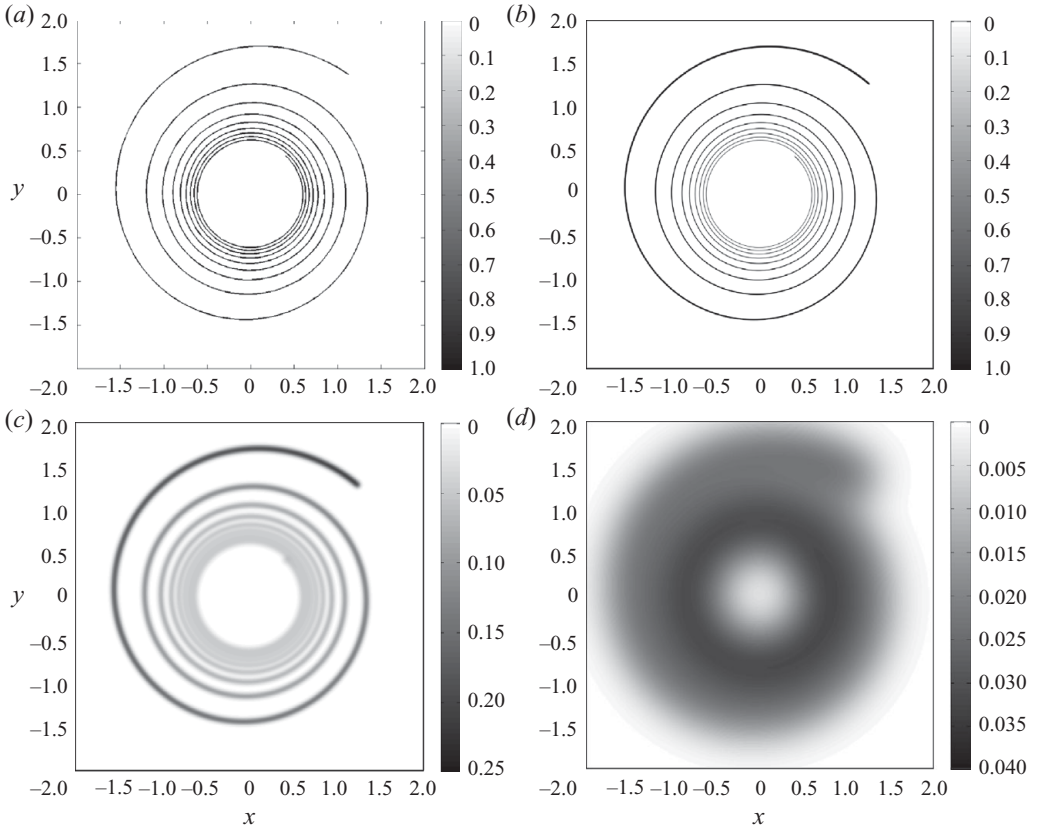

FIGURE 5. Spiral of scalar created by the roll-up of a strip around a point vortex with a circulation $\Gamma = 14.2$ cm^2 s^{-1} at $t = 10$ s. The diffusivity is equal to (*a*) $D = 10^{-8}$ cm^2 s^{-1}, (*b*) $D = 10^{-6}$ cm^2 s^{-1}, (*c*) $D = 10^{-4}$ cm^2 s^{-1} and (*d*) $D = 10^{-2}$ cm^2 s^{-1}. The scalar is injected initially along the x-axis with 0.6 cm $< x <$ 1.8 cm. The initial thickness of the strip is $s_0 = 0.11$ cm. In (*a*), the strip is plotted as a line, whereas in (*b–d*), it is reconstructed on a two-dimensional mesh.

decreased at some locations close to the vortex centre. Since the stretching is larger at the centre than at the periphery, the diffusion is faster and the concentration smaller there. This is very similar to the experimental result of Meunier & Villermaux (2003) except that here the strip contains more turns because the scalar is located closer to the vortex centre. For even larger diffusivities ($D = 10^{-4}$ cm^2 s^{-1}), the scalar has a much lower concentration (note the change in the colourbar) and the strip starts to mix with itself at the centre of the vortex. At a very high diffusivity ($D = 10^{-2}$ cm^2 s^{-1}), the aggregation of the strip is generalized to the whole area, which creates a ring of scalar. The scalar has a higher concentration close the centre, since it is spread on an area smaller that at the periphery (proportional to the radius). It can be noted that the numerical simulation describes well (at least qualitatively at this stage) the aggregation of the strip. However, we expect the ring to become a single circular patch at even larger diffusivities (without a hole at the centre), but this case cannot be described by the model since it corresponds to a thickness of the strip of the order of the curvature radius.

To compare the numerical results quantitatively with the experiment, we have plotted the maximal concentration as a function of the radius in figure 6(*a*). The

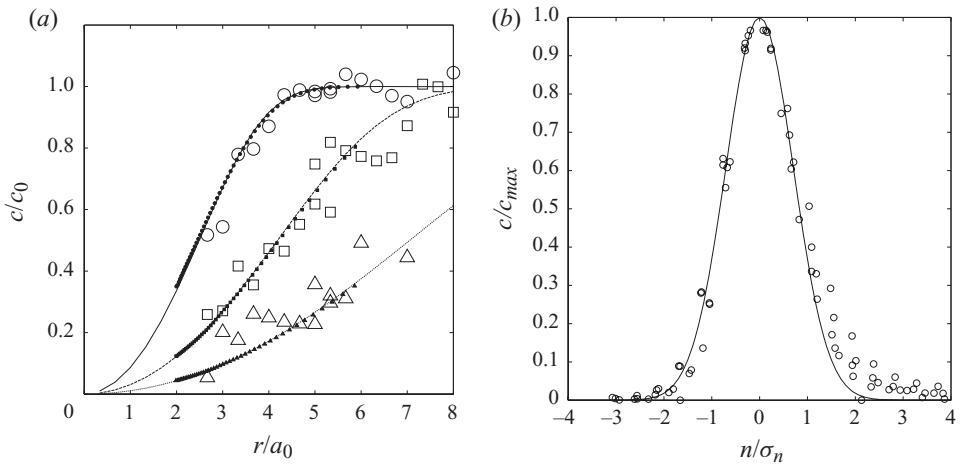

FIGURE 6. (*a*) Maximal concentration of the scalar along the strip as a function of the radius at $t = 5$ s (circles), $t = 10$ s (squares) and $t = 20$ s (triangles). Experimental data (open symbols) and theoretical predictions (lines) are taken from Meunier & Villermaux (2003). Numerical results (black filled symbols) are obtained with a diffusivity ($D = 5 \times 10^{-6}$ cm^2 s^{-1}). The experimental vortex core size a_0 is equal to 0.3 cm. (*b*) Transverse profile of the scalar as a function of the coordinate normal to the strip. Symbols are taken from the experimental data published in Meunier & Villermaux (2003) at $t = 20$ s and are compared to a Gaussian function (solid line).

numerical values (plotted as small black symbols) are in excellent agreement with the experimental and theoretical data taken from Meunier & Villermaux (2003, figure 4a). However, for this figure, the maximal concentration has been taken equal to $c_0\mathrm{erf}(1/\sqrt{4\tau})$ instead of $c_0/\sqrt{1+4\tau}$ as in (2.8) since it is the solution for a square initial transverse profile with a width $2s_0$. The numerical values are slightly smaller than the theory at large r and slightly larger for small r. But this error remains smaller than 3 % and might be due to numerical errors during the advection of the tracers $\boldsymbol{x}_i$. We have also checked that the experimental transverse profile is Gaussian, as predicted by (2.7). It is plotted in figure 6(*b*) and is indeed very close to Gaussian although it is slightly asymmetric (larger for $n > 0$). This might be due to a misalignment of the camera with the axis of the vortex, which makes visible the dye which is behind the illuminated sheet of dye, thus enlarging the thickness of the strip for $n > 0$. We now use this method to study a more complex flow, where no analytical solution is available.

3. Mixing in a sine flow

In the rest of the paper, we will analyse a case study of mixing at high Péclet number, taking advantage of the new numerical technique of strip diffusion. The aim is to link the local properties of stretching enhanced diffusion of a strip well captured by the numerical technique, to the global properties of the mixture such as spectra and PDF for a prototype chaotic flow to understand, using this new tool, how the complex mixture at a given stage of its development has been built from elementary objects (the stretched strips) and an appropriate interaction rule.

3.1. *Definition of the sine flow*

We have chosen to analyse the case of a sine flow, since it has been commonly studied (Alvarez *et al.* 1998; Cerbelli *et al.* 2004; Thiffeault, Doering & Gibbon 2004) using several numerical methods (tracking of tracers and spectral methods).

m	0	1	2	3	4	5	6
χ^x	1.2154	4.2865	1.9023	3.4034	0.9480	4.3850	2.3774
χ^y	3.1199	5.6534	5.1624	4.0521	5.1395	4.1483	2.1487

TABLE 1. Phases of the sine flow in the x- and y-direction at each period m.

Moreover, it is well known for its chaotic mixing behaviour at high enough velocities. The sine flow (or random wave flow, Zeldovich 1982) consists of alternating vertical and horizontal sinusoidal shear flows. The randomness of the flow is introduced via phases χ^x and χ^y, which are chosen randomly at each period (Thiffeault *et al.* 2004), defining the flow as

$$(v_x, v_y) = V_0 \left[0, \sin(2\pi x + \chi_m^x)\right] \quad \text{for } m < t < m + 1/2, \tag{3.1}$$

$$(v_x, v_y) = V_0 \left[\sin(2\pi y + \chi_m^y), 0\right] \quad \text{for } m + 1/2 < t < m + 1, \tag{3.2}$$

where the integer m is the period number, t is time and the amplitude of the flow V_0 is chosen equal to $1/\sqrt{2}$ in order to be in a chaotic regime (see Alvarez *et al.* 1998). The phases are chosen randomly between 0 and 2π. Their values are given in table 1. By chaotic, we mean that the flow will not leave room for segregated, unmixed islands at long times and that, although the flow will generate a non-trivial concentration distribution $P(c)$ (defined in § 6), that distribution will ultimately converge towards a Dirac delta centred around the average concentration $\langle c \rangle$

$$P(c) \underset{t\to\infty}{\longrightarrow} \delta(c - \langle c \rangle), \tag{3.3}$$

that is, in the language of Ergodic theory, towards a measure of uniform probability over the whole domain. In that sense, the flow in (3.2) is mixing (Arnold & Avez 1967).

A strip of scalar is introduced at $t = 0$ along the x-axis between $x = -0.5$ and $x = +0.5$. The initial transverse profile is supposed to be Gaussian ($c(y) = c_0 \mathrm{e}^{-y^2/s_0^2}$) with an initial thickness equal to $s_0 = 0.05$. The evolution of the scalar is governed by the advection–diffusion equation (1.2) where the diffusivity D defines the Péclet number as

$$Pe = 1/D, \tag{3.4}$$

meaning that the length scale is chosen equal to the wavelength (equal to 1), and the typical velocity is chosen equal to $V_0\sqrt{2}$.

3.2. *Temporal evolution*

Figure 7 shows the distributions of scalar at various times for a moderate Péclet number ($Pe = 10^5$). The strip, initially straight, is bent and stretched by the flow. After one period, its thickness has decreased due to the compression in its transverse direction. However, the maximal concentration is still equal to the initial concentration c_0 since the mixing time has not yet been reached. After two periods, the scalar has started to diffuse, leading to a grey shade of the strip. This diffusion is a proof that the mixing time has been reached, i.e. that the dimensionless time τ is of the order of one or larger. The strip is thinner than after one period, and several parts of the strip get closer to each other. However, there is no reconnection of the strip with itself.

After four periods (figure 7*c*), the strip has a very disordered shape. It is bent in many places and contains a few cusps. Different parts of the strip are so close that they have mixed because of diffusion. It is almost invisible except at the locations

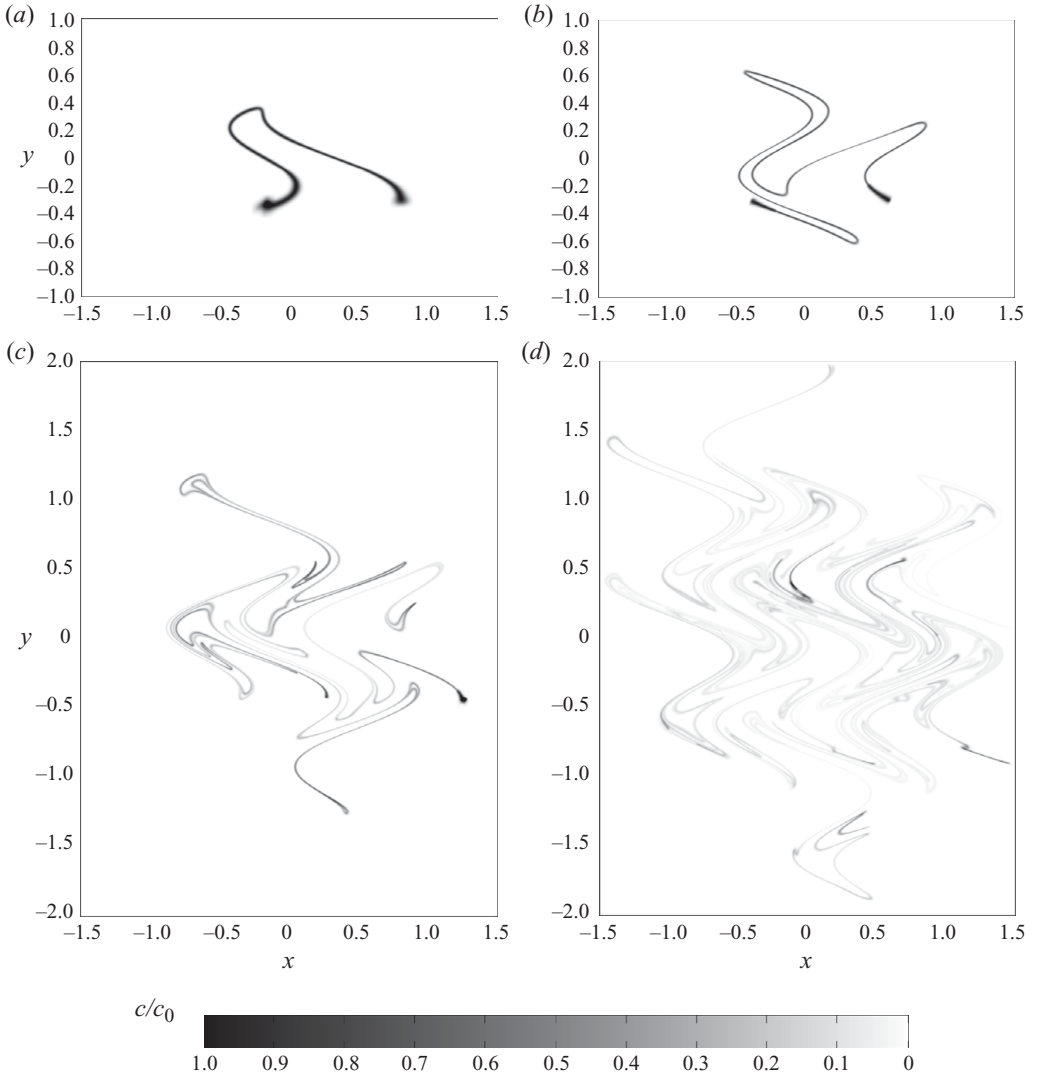

FIGURE 7. Temporal evolution of a strip of scalar in a sine flow for a Péclet number equal to 10^5. The fields of the scalar are given at (*a*) $t=1$, (*b*) $t=2$, (*c*) $t=4$ and (*d*) $t=7$.

where the different parts separate, as can be seen at the upper left loop ($x=-0.7$, $y=1.2$). The concentration of the scalar becomes smaller and smaller, and there are no remaining parts still bearing the initial concentration c_0. The thickness of the strip remains blocked at the Batchelor scale $\sqrt{D/\gamma}$ (see (2.12)), γ being the average stretching rate of the strip, as soon as diffusion balances substrate compression.

After seven periods (figure 7*d*), the strip has been bent and reconnected many times. It spreads on a large domain and very well shows the chaotic behaviour of the flow. The concentration is very small, such that the scalar is almost completely diluted in the surrounding medium.

3.3. *Influence of the Péclet number*

The main advantage of the strip diffusion method is that the diffusivity can be varied *a posteriori* by simply tuning the dimensionless time τ accordingly. It is thus

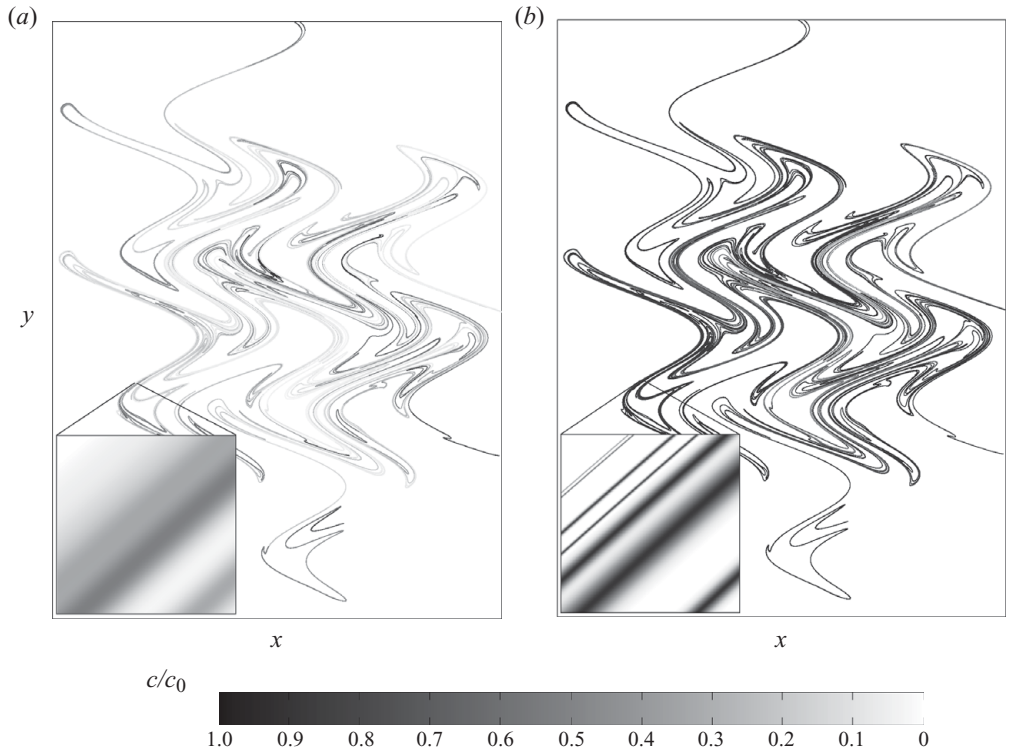

FIGURE 8. Distribution of a scalar in a sine flow at $t = 7$ for (*a*) $Pe = 10^7$ and (*b*) $Pe = 10^{10}$. Due to a lack of printing resolution, the thickness of the strip has not been respected: the strip has been plotted as a line. However, the image has been zoomed 200 times in the inset to show the correct thickness of the strips.

extremely easy to plot the distributions of scalar at any diffusivity (as high as wished in particular). Two examples are given in figure 8 for $Pe = 10^7$ and $Pe = 10^{10}$. Such numerical simulations are impossible to do using a spectral code, since the number of points needed would be too high. Indeed, it was impossible to reconstruct the scalar field on a two-dimensional mesh, and the strip has only been plotted as a line in figure 8. However, it is possible to reconstruct the scalar field in two dimensions on a smaller area. This is shown in the insets of figure 8 and proves that the results are correct although it is impossible to visualize them on the whole field.

At a Péclet number equal to 10^7, the strip has reached the mixing time in some places, but some parts of the strip seem to have a concentration equal to c_0. The inset shows that the strip has reconnected with itself, leading to a rather blurry picture. On the contrary, for $Pe = 10^{10}$, the different parts of the strip remain separate, even at the upper left corner of the inset, where two lines are not only extremely close, but also extremely thin. This is in agreement with the fact that the mixing time has not been reached there, which prevents the reconnection of the strip (due to the flow incompressibility). At such a high Péclet number, the mixing time has not been reached almost everywhere, and the concentration is equal to c_0 almost everywhere. It is clear on this figure that the spatial distribution of scalar is very complex and contains a lot of information, which is why the numerical simulation gets very slow at these late stages. We are using this information in the following to analyse the mixing properties of the flow and relate them to the stretching of the strip.

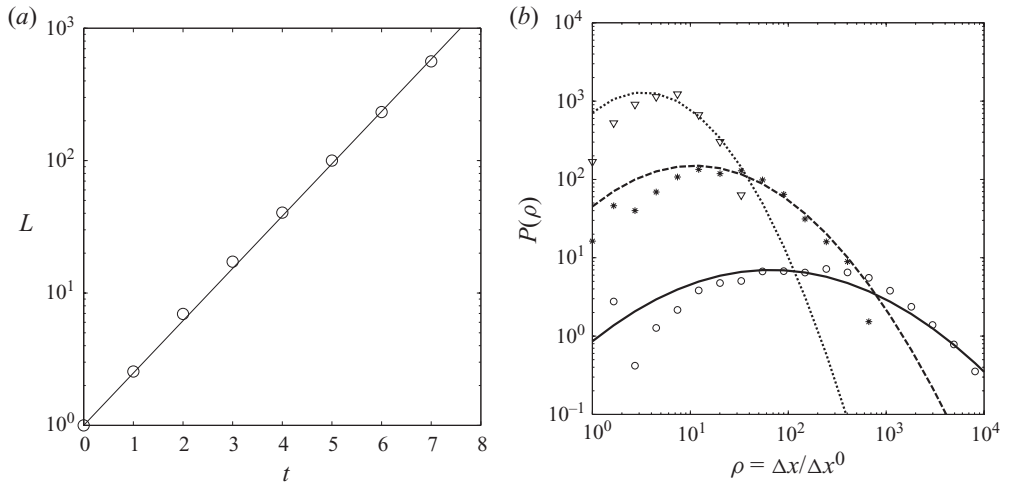

FIGURE 9. (*a*) Total length of the strip as a function of time. The solid line corresponds to an exponential growth with a mean stretching rate $\gamma = 0.91$. (*b*) PDF of elongation of the strip for $t = 2$ (∇, dotted line), $t = 4$ ($*$, dashed line) and $t = 7$ ($\circ$, solid line). Lines correspond to the theoretical prediction of (4.14).

4. A simple model of stretching

4.1. *Temporal evolution of the strip length*

It is well known that in a chaotic stirring flow sustaining a series of stretchings and foldings, a strip of scalar is stretched exponentially in time: this is the paradigm of the Baker transform (Ottino 1989). More generally, a succession of random motions distributed in intensity and direction results in a global exponential lengthening of material lines (Kraichnan 1974; Duplat & Villermaux 2000). This is very well-confirmed in the present sine flow, where the total length L of the strip increases as $e^{\gamma t}$, as shown in figure 9. The numerical value of the mean stretching rate (also called topological entropy) can be obtained accurately $\gamma = 0.91 \pm 2\,\%$. This value will be the only constant needed for the theory developed in the following.

4.2. *PDF of stretching factors*

The total length of the strip is a global characteristic which does not give any information about the variation of the elongation ρ along the strip, which is distributed according to a well-defined PDF, $P(\rho)$. It is defined as the probability of finding a point on the final strip, where the strip has been stretched by a factor $\rho = \Delta x/\Delta x^0$. Since the final refinement is done such that the tracers are equally spaced along the strip, $P(\rho)$ is easily calculated as the number of tracers for which $\Delta x/\Delta x^0$ is in the interval $[\rho,\ \rho + \mathrm{d}\rho]$ divided by $\mathrm{d}\rho$. These PDF are plotted for $t = 2$, 4 and 7 in figure 9. The numerical results seem to be parabolic in this logarithmic scale, which means that $P(\rho)$ is a Gaussian function of $\log(\rho)$. It is clear that the parabola get wider as time increases. Moreover, $\log(\rho_M)$ increases linearly in time, where ρ_M is the most probable stretching.

4.3. *Multi-step stretching*

The above result and shape of $P(\rho)$ is readily understood. Let us split the stretching of the strip at one point into N successive random stretching operations. We assume that a given tracer of the strip experiences a stretching ρ_1 between $t = 0$ and $t = \delta t$, a

stretching ρ_2 between $t=\delta t$ and $t=2\delta t\ldots$ The total stretching ρ of the strip after N operations is thus the product of the elementary stretchings: $\rho=\prod\rho_i$. If we assume that the stretching operations are random and independent, the stretching rate ρ has a log-normal law in virtue of the central limit theorem. This means that the probability $Q(\rho)$ that a point on the initial strip is stretched by a factor ρ is given by $Q(\rho)=\exp[-(\log\rho-N\mu)^2/2N\sigma^2]/\rho\sqrt{2\pi N\sigma^2}$, where μ and σ^2 are the mean and variance of $\log\rho$. However, the probability $P(\rho)$ that a point on the final strip has experienced a stretching ρ is equal to $(L_0/L(t))\,\rho\,Q(\rho)$ because the elementary length of such an interval has been multiplied by ρ, thus weighting the probability by a factor ρ. Since the number N of elementary stretchings is proportional to the time t in a permanently stirred flow, one can rewrite the probability $P(\rho)$ as

$$P(\rho)=\frac{L_0/L(t)}{\sqrt{4\pi\kappa t}}\exp\left[-\frac{(\log\rho-\gamma_p t)^2}{4\kappa t}\right], \tag{4.1}$$

where $\gamma_p=N\mu/t$ is the most probable stretching rate (i.e. the most probable finite time Lyapunov exponent), κ reflects the diffusion of the stretching factors and is such that $\sigma^2=2\kappa t/N$. This result is equivalent to the one derived, also assuming that the stretching is operated in multiple discrete steps, by Kalda (2000) who showed that the probability $P(\log\rho)$ is the solution of a diffusion–advection equation

$$\frac{\partial P}{\partial t}+\gamma_p\frac{\partial P}{\partial\log\rho}=\kappa\frac{\partial^2 P}{(\partial\log\rho)^2}, \tag{4.2}$$

The advective term $\gamma_p\partial P/\partial(\log\rho)$ corresponds to a constant average stretching of the strip meaning that the average of the logarithm of the strip length $\log\rho$ increases with time as $\gamma_p t$. The diffusive term $\kappa\partial^2 P/(\partial\log\rho)^2$ comes from the distribution of the stretching intensities in the flow, which is progressively explored by the strip as time progresses. Indeed, a subpart of the strip can be stretched at a rate slower or faster than γ_p, and this alternatively and randomly as time evolves. The net result is a diffusion of an initial stretching $\log\rho$ to neighbouring stretchings, with an apparent rate κ reflecting the width of the distribution of the stretching rates.

4.4. *Link with stochastic processes*

An interesting analogy can also be drawn with the dynamics of pair dispersion in random flows. Let $r(t)$ be the distance between two material points constitutive of the strip. There is, in general, a deterministic part of the rate of elongation of $r(t)$ given by the structure of the mean flow and boundary conditions, plus a random contribution due to the hieratic/chaotic nature of the motion. For smooth flows (those characteristic of the so-called Batchelor régime, a régime in which the sine flow is likely to fall), the velocity gradient $|\nabla\boldsymbol{v}|$ is approximately constant over the domain, and thus the typical velocity difference $|\delta v(r)|$ is expected to increase in proportion to r itself. The rate of increase of r is in proportion to the number of degrees of freedom offered by the flow, that we denote d, like the dimension of space. The contribution of this deterministic part to the net elongation of r will thus be dr. Now, the chaotic motions generated by the flow itself impact the increase of r as well. Those may affect the elongation of r with a probability proportional to its length r itself. We call it $rf(t)$ where $f(t)$ is, in the simplest case, chosen as a Brownian white noise with zero mean, broad variance, and uncorrelated with itself from one flow cycle to the other.

We thus choose to examine the following model for the distance $r(t)$ between two particles:

$$\dot{r} = r\,(d + f(t)), \tag{4.3}$$

$$\langle f(t)\rangle = 0 \quad \text{and} \quad \langle f(t)\, f(t')\rangle = \mathscr{D}\,\delta(t - t'), \tag{4.4}$$

where $\langle\cdot\rangle$ stands for the average over the noise realizations $\langle\cdot\rangle = \int(\cdot)\,B(f)\,\mathrm{d}f$ with $B(f)$ a centred broad distribution. Time t is made dimensionless with a suitable stretching rate γ_0. Let $Q(r,t)$ be the distribution of distances r between material particles along a strip at time t. It corresponds to the probability $Q(\rho,t)$ that a strip has been stretched by a factor ρ at time t. This identity is legitimate in smooth flows where stirring is dominated by a single length scale and where no small scale activity in the underlying velocity field contributes to the wrinkling of an advected material line. This result is no longer true in rough, multiscale flows (Villermaux & Gagne 1994). One has obviously

$$Q(r, t + \Delta t) = \int B(f)\,\mathrm{d}f\; Q(r - \Delta r, t), \tag{4.5}$$

the increments Δr and Δt being linked through the dynamics in (4.3). A Taylor expansion of (4.5) leads, according to Itô rules (expressing that the jump rates of Δr are determined at the starting point at time t, see Van Kampen 1981; Gardiner 2003), to the corresponding Fokker–Planck equation for $Q(r,t)$

$$\frac{\partial Q}{\partial t}\Delta t = -\frac{\partial}{\partial r}\left(Q\langle\Delta r\rangle\right) + \frac{1}{2}\frac{\partial}{\partial r^2}\left(Q\langle(\Delta r)^2\rangle\right). \tag{4.6}$$

Computing the mean increment $\langle\Delta r\rangle$ and its variance $\langle(\Delta r)^2\rangle$ according to (4.3) and (4.4) gives

$$\langle\Delta r\rangle = (d + \mathscr{D})\, r\,\Delta t, \tag{4.7}$$

$$\langle(\Delta r)^2\rangle = 2\,\mathscr{D}\, r^2 \Delta t, \tag{4.8}$$

providing finally (see also Graham & Schenzle 1982)

$$\frac{\partial Q}{\partial t} + (d + \mathscr{D})\frac{\partial(r\,Q)}{\partial r} = \mathscr{D}\,\frac{\partial^2(r^2 Q)}{\partial r^2}, \tag{4.9}$$

or, if instead of $Q(r,t)$, one is interested in $P(\log r, t)$ which is such that $P(\log r, t) = r\,Q(r,t)$, one has

$$\frac{\partial P}{\partial t} + d\,\frac{\partial P}{\partial \log r} = \mathscr{D}\,\frac{\partial^2 P}{\partial(\log r)^2}. \tag{4.10}$$

Equation (4.10) is formally identical to (4.2), and equal to it when $d\gamma_0 = \gamma_p$ (remember that $t \equiv \gamma_0 t$ in (4.3)) and $\mathscr{D}\gamma_0 = \kappa$. When $\mathscr{D} = 1$, that is when the noise has the same weight as the deterministic part of the flow, one expects that

$$\gamma_p = d\,\kappa, \tag{4.11}$$

in dimension d, a relationship which has the interesting consequence that the parameters describing the stretching field of the flow (γ_p, κ) in (4.2) reduce to a single parameter. It can be noted that J. Kalda (personal communication, 2008) has given a straightforward way to derive (4.11) by considering a space-filling stationary flow in a closed box for which $P(r) \sim r^d$ and relating it to the stationary solution $P(r) \sim r^{\gamma_p/\kappa}$ of (4.2).

Under the condition (4.11) above, the flow dispersion properties being characterized by a single parameter, it is natural to wonder whether $Q(r,t)$ (or $P(\log r,t)$) can be interpreted as resulting from a scale dependent diffusive process with an effective scale dependent diffusivity $D(r)$, as the one imagined by Richardson for pair dispersion in random flows (Richardson 1926). The above transport equation for $Q(r,t)$ does not coincide with Richardson's transport equation for the distribution of the distance r between pairs of particles, but its density $q(r,t)$ such that, for an isotropic d-dimensional field $Q(r,t)\,\mathrm{d}r \sim r^{d-1}q(r,t)\,\mathrm{d}r$, does. One checks indeed that (4.9) coincides with (see e.g. Monin & Yaglom 1975; Falkovich, Gawedzki & Vergassola 2001)

$$\frac{\partial q(r,t)}{\partial t} = \frac{1}{r^{d-1}}\frac{\partial}{\partial r}\left[D(r)\,r^{d-1}\frac{\partial q(r,t)}{\partial r}\right], \tag{4.12}$$

for $\mathscr{D}=1$, provided the diffusivity $D(r)$ can be written (in dimensional units)

$$D(r) = \gamma_0 r^2. \tag{4.13}$$

This scaling for the diffusivity $D(r)=|\delta v(r)|\,r$ is consistent with the expectation in smooth flows such as the Batchelor régime for which $|\delta v(r)|=\gamma_0 r$. The log-normal distribution for the stretchings in (4.1) thus simply results from a succession of uncorrelated motions.

4.5. *Conclusion*

A direct consequence of the stretching model above is that the length of the strip increases exponentially in time (since $L(t)=L_0\int \rho\, Q(\rho,t)\,\mathrm{d}\rho$), with a mean stretching rate equal to $\gamma=\gamma_p+\kappa$. Using this relation and the link between γ_p and κ in (4.11) for $d=2$ (two dimensions), one can give explicitly the constants of the model as a function of the mean stretching rate γ, which has been determined numerically accurately. The model does not contain any fitting parameter any more. The probability $P(\rho)$ that a point on the final strip has been stretched by a factor ρ is given by

$$P(\rho) = \frac{\mathrm{e}^{-\gamma t}}{\sqrt{4\pi\gamma t/3}}\exp\left[-\frac{(\log\rho - 2\gamma t/3)^2}{4\gamma t/3}\right]. \tag{4.14}$$

This law is plotted in figure 9 at various times. The agreement with the numerical simulations is fair. In particular, the most probable stretching factor is correctly predicted as a function of time, since a best fit gives a most probable stretching rate $\gamma_p=0.7\approx 2\gamma/3=0.6$, as expected from the model. The broadening of the PDF is also fairly well-predicted, a best fit gives a diffusivity $\kappa=0.22$ instead of $\kappa=\gamma/3=0.3$ from the model. This result suggests that the hypothesis made in (4.11) is fairly consistent with the data.

We now use this model to infer global quantities of the concentration field, which we compare to the simulation.

5. Spectrum of the scalar

We analyse the energy spectra of the scalar advected by the sine flow presented in § 3, and relate them to known results and issues.

5.1. *Construction of the spectrum*

The one-dimensional energy spectrum $\Gamma(k)$ of the scalar is defined (see e.g. Batchelor 1959) as the total two-dimensional spatial spectrum $\Phi(\boldsymbol{k}')/2$ contained in an annulus

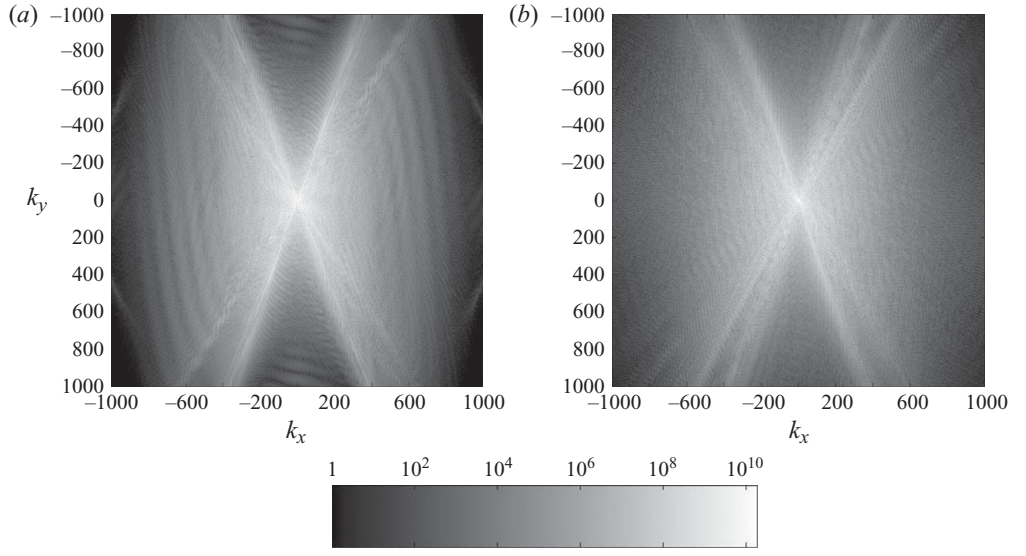

FIGURE 10. Two-dimensional energy spectrum $\Phi(\boldsymbol{k})$ of the scalar at (*a*) $t=4$ and (*b*) $t=7$ for $Pe=10^5$. The spectrum is calculated by a two-dimensional FFT of the scalar spatial distribution $c(x)$. The grey map is logarithmic in order to visualize large wavenumbers (corresponding to very small values of energy).

of width dk divided by dk

$$\Gamma(k)\,\mathrm{d}k = \int\int_{k<||\boldsymbol{k}'||<k+\mathrm{d}k} \frac{1}{2}\Phi(\boldsymbol{k}')\,\mathrm{d}\boldsymbol{k}'. \tag{5.1}$$

The spatial spectrum $\Phi(\boldsymbol{k})$ is usually defined as the Fourier transform of the auto-correlation function of the scalar $\langle c(\boldsymbol{x})c(\boldsymbol{x}+\boldsymbol{r})\rangle_{\boldsymbol{x}}$. However, it is also equal to the squared modulus of the Fourier transform $\tilde{c}(\boldsymbol{k})$ of the scalar, due to the properties of the auto-correlation function

$$\Phi(\boldsymbol{k}) = \frac{1}{4\pi^2}\int\int_{-\infty}^{+\infty} \mathrm{e}^{-\mathrm{i}\boldsymbol{k}\cdot\boldsymbol{r}}\langle c(\boldsymbol{x})c(\boldsymbol{x}+\boldsymbol{r})\rangle_{\boldsymbol{x}}\,\mathrm{d}\boldsymbol{r} = \frac{4\pi^2}{\mathscr{A}}|\tilde{c}(\boldsymbol{k})|^2, \tag{5.2}$$

where $\mathscr{A}$ is the total area of the domain of the simulation. Numerically, it is easy to compute the two-dimensional energy spectrum $\Phi(\boldsymbol{k})$ from the fast Fourier transform (FFT) of the scalar distribution $c(\boldsymbol{x})$, which has been reconstructed on a two-dimensional grid. This spectrum is shown in figure 10 at different times. The spectrum is extremely peaked around 0, and the grey map has been chosen logarithmic in order to visualize large wavenumbers (corresponding to very small values of energy). This spectrum is shown in figure 10 for different times. The spectrum is extremely peaked around 0, and exhibits rays of high energy oriented at about $\pm 60^\circ$ with respect to k_x. This indicates that the strips are mainly oriented at $\mp 30^\circ$ with respect to x, as can be seen in figure 7(c,d). This means that the flow is not completely isotropic and has two dominant stretching directions. Using this two-dimensional spectrum, the one-dimensional spectrum is then calculated by integration on an annulus of width dk. However, this method is very demanding in memory since it creates a two-dimensional matrix of the scalar, whereas the strip is defined on a one-dimensional vector.

An alternative way is to use the fact that the scalar distribution is defined as a sum of ellipses with a Gaussian shape as can be seen in (2.14). Since the Fourier transform

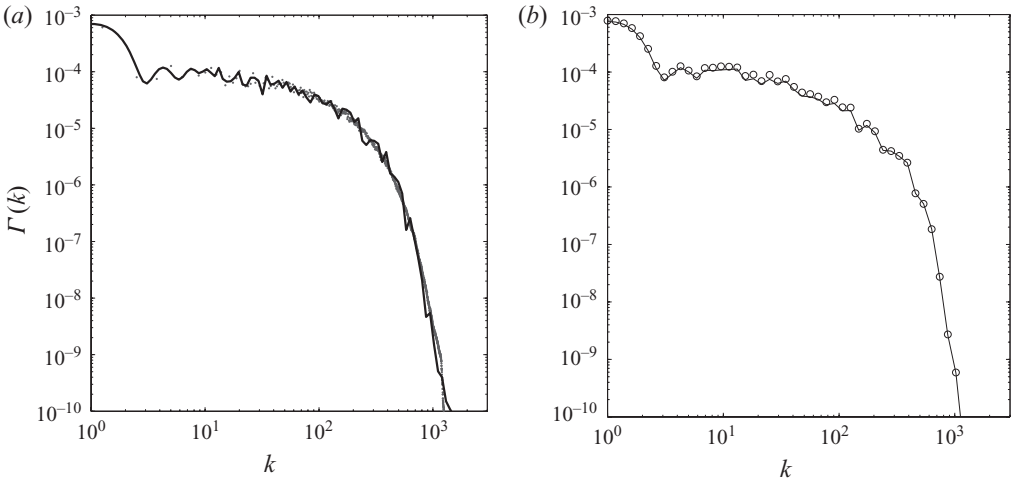

FIGURE 11. Energy spectrum of the scalar at $t = 7$ for $Pe = 10^5$. (*a*) The spectrum is calculated by FFT of the scalar spatial distribution (grey symbols) and directly by integration along the strip using (5.3) (black solid line). (*b*) The spectrum is calculated using (5.3) with post-treatment of the cusps (solid line) and without post-treatment of the cusps (○).

of a Gaussian is Gaussian, one can calculate directly $\tilde{c}(k)$ from (2.14) as a sum over the tracers $\boldsymbol{x}_i$ (using a change of variable $\boldsymbol{x}' = \boldsymbol{x} - \boldsymbol{x}_i$ in the integral over $\boldsymbol{x}$):

$$\tilde{c}(\boldsymbol{k}) = \sum_i \frac{c_0 \Delta l s_i}{4\pi \times 1.7726} \, \mathrm{e}^{-(\boldsymbol{k}\cdot\tilde{\boldsymbol{\sigma}}_i)^2 \Delta l^2/4} \, \mathrm{e}^{-(\boldsymbol{k}\cdot\tilde{\boldsymbol{n}}_i)^2 s_i^2 (1+4\tau_i)/4} \, \mathrm{e}^{-\mathrm{i}\boldsymbol{k}\cdot\boldsymbol{x}_i}. \tag{5.3}$$

We recall that $\tilde{\boldsymbol{\sigma}}_i$ and $\tilde{\boldsymbol{n}}_i$ are the unit vectors tangent and normal to the strip, respectively, Δl is the distance between two tracers, s_i is the striation thickness and τ_i is the dimensionless time. Since $\tilde{c}(\boldsymbol{k})$ is here given by an analytical expression (and not a matrix), it is very simple to calculate the spectrum at a given wavenumber k by integrating on a circle in the two-dimensional wavevector coordinates

$$\Gamma(k) = k \int_{\theta=0}^{\theta=2\pi} |\tilde{c}(k\cos\theta, k\sin\theta)|^2 \, \mathrm{d}\theta. \tag{5.4}$$

In our simulations, this formula is discretized on 20 or 50 angles θ, depending on the accuracy needed. The main advantage of this method is that it calculates the energy spectrum at each wave number k independently, unlike the method using a numerical FFT of the scalar distribution. The need in memory is thus very low and the spectra can be calculated on as many decades as wanted. Moreover, the distribution of wave numbers can be chosen exponential, which is very interesting for spectra in logarithmic scale.

An example of a spectrum is plotted in figure 11 using the two numerical methods described above. The method using an FFT of the reconstructed two-dimensional scalar field (plotted as symbols) is particularly good at large wavenumbers, since the integration over the annulus of width dk contains many numerical data at large k (leading to an efficient averaging). However, this method gives very few points at low wave number, since k is a multiple of $2\pi/\mathscr{L}$, where the size of the domain $\mathscr{L}$ cannot be taken too large. This method can only give the spectrum over three decades, since the maximum size of a two-dimensional matrix is 4096^2.

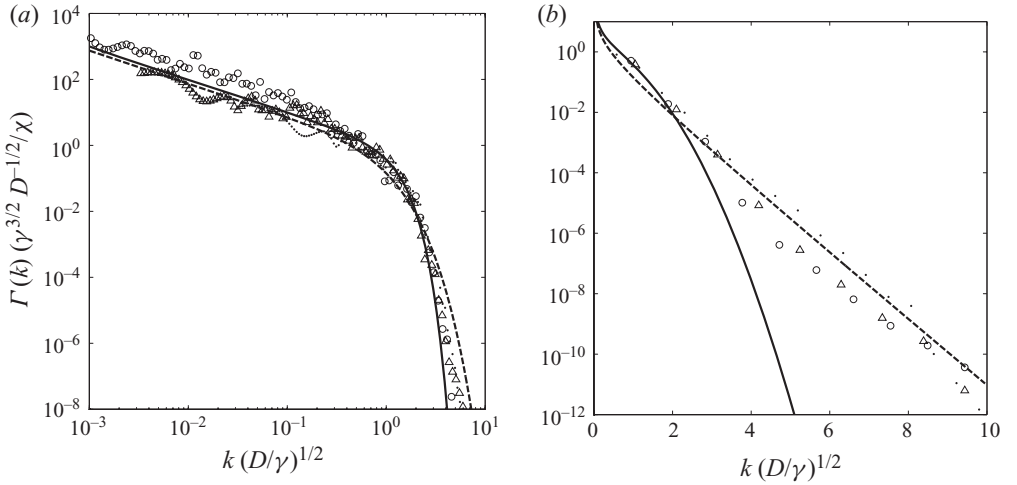

FIGURE 12. Energy spectrum of the scalar at $t = 7$, in a simulation where a new strip of scalar is injected at $t = 0, 1, 2, 3, 4, 5, 6$, to mimic sustained turbulence. The Péclet number is equal to $Pe = 10^3$ (•), $Pe = 10^5$ (△) and $Pe = 10^7$ (○). The solid line corresponds to the Batchelor spectrum (5.5) and the dashed line corresponds to the solution (5.8) proposed by Kalda (2000) for sustained turbulence. The scale for the wavenumber is (*a*) logarithmic and (*b*) linear.

The method based on an analytical value of $\tilde{c}(k)$ is very efficient at low wave number: it gives an almost continuous description of the spectrum, due to the very dense amount of data at low k. At high wavenumber, there seem to be some numerical oscillations of the spectrum compared to the other method. This comes from the limited number of angles θ in the discretization of the integration over an annulus, and can be reduced by using more angles (up to 200 angles). The agreement between the two methods is excellent, which validates the second method. In the following, we will use this alternative method only since it is faster and more accurate. We have also checked the post-treatment of the cusps introduced in § 2.5 has a negligible influence on the spectrum. This effect is hardly visible in figure 11(*b*) where the spectrum is plotted with and without post-treatment of the cusps. We are thus confident of the fact that the method failing at the cusps has a negligible influence on this global quantity.

5.2. *Spectrum of a forced scalar*

Figure 12 shows the energy spectrum of a scalar in a sine flow for three different Péclet numbers. A new strip of scalar has been injected at each period of the sine flow to mimic forced turbulence and reach a stationary state. This procedure has been used only in this subsection because spectra have been extensively studied in the regime of forced turbulence rather than in decaying turbulence. In this way, there is a constant injection of energy at low wavenumber, which is transferred to high wavenumbers by a direct cascade. This is consistent with the mechanism presented by Batchelor (1959): the wavenumbers increase, due to the stretching of the strip, up to the scale where the scalar is dissipated (see (2.12)). In this picture where the scalar variance is conserved as k increases, the spectrum of a scalar is given by

$$\Gamma(k) = \frac{\chi}{\gamma k} \mathrm{e}^{-Dk^2/\gamma}, \tag{5.5}$$

a result which holds for smooth flows characterized by a single mean stretching rate γ and the dissipation rate χ

$$\chi = 2D \int_0^\infty k^2 \Gamma(k)\, \mathrm{d}k. \tag{5.6}$$

This prediction is plotted in figure 12 as a solid line. It is in excellent agreement with the numerical results, which present a k^{-1} spectrum on three decades in the so-called viscous–convective subrange (above the Batchelor scale). This clear evidence is possible since the Péclet number is high (up to 10^7). It is less clear on the simulations made at small Péclet number ($Pe = 10^3$), where the slope k^{-1} is hardly visible on one decade.

At high wavenumbers, the spectrum presents a cut-off around the Batchelor wavenumber $\sqrt{\gamma/D}$. However, the numerical results lie above the Batchelor spectrum (5.5) at high wavenumber. This disagreement is even more visible when plotting the spectrum using a linear scale for the wavenumber (figure 12*a*). The numerical results show that the spectrum has an exponential decay e^{-k} instead of e^{-k^2}. This exponential behaviour is consistent with Kraichnan (1974) who generalized the result of Batchelor (1959) to the case of a random stretching field, leading to an exponential decay of the spectrum (see also Toussaint *et al.* 2000 and Yeung, Xu & Sreenivasan 2002). This is qualitatively understood by the fact that a distribution of stretching rates γ leads to a distribution of Batchelor scales $\sqrt{D/\gamma}$, thus broadening the spectrum at high wavenumbers in a continuous fashion, and thus stretching the cutoff from e^{-k^2} to e^{-k}. This result can be recovered in a simple way by using (4.2) for the PDF of stretching rate $P(\rho)$, as proposed by Kalda (2000). Indeed, in the absence of diffusion, the quantity $k\Gamma(k)$ remains unchanged during the stretching by the flow, whereas the wavenumber is multiplied by the same amount as the stretching factor ρ. The PDFs of stretching rate and $k\Gamma$ are thus governed by the same differential equation (4.2). However, the presence of diffusion adds a decaying term in the equation for $k\Gamma$ with a decay rate equal to $-2Dk^2$, which leads to the following equation for $k\Gamma$:

$$\frac{\partial(k\Gamma)}{\partial t} + \frac{2\gamma}{3}\frac{\partial(k\Gamma)}{\partial(\log k)} = \frac{\gamma}{3}\frac{\partial^2(k\Gamma)}{\partial(\log k)^2} - 2Dk^2(k\Gamma). \tag{5.7}$$

As explained in § 4, γ is the mean stretching rate of the strip, and has been calculated numerically very accurately for the sine flow ($\gamma = 0.91$). The stationary solution of this equation is given by a Hankel function of order one (see Kalda 2000)

$$\Gamma(k) = A H_1^{(1)}\left(\mathrm{i}k\sqrt{6D/\gamma}\right), \tag{5.8}$$

where $A = H_1^{(1)}(\mathrm{i}\sqrt{6D/\gamma})^{-1}$. This solution scales as $k^{-1}\mathrm{e}^{-k\sqrt{6D/\gamma}}$ at high wavenumbers, i.e. for $k \ll \sqrt{\gamma/D}$. This exponential decay corresponds to the result predicted by Kraichnan (1974) and is now tightly linked to the distribution of stretchings itself. This solution (5.8) is plotted in figure 12 as a dashed line. It is, as expected, in very good agreement with the numerical results at small wavenumbers (since it decays as k^{-1} like the Batchelor spectrum). It is also in excellent agreement at higher wavenumbers, as can be seen in figure 12(*b*), where the scale of the wavenumber is linear.

It might be surprising that the spectrum has an exponential decay at late stages. Indeed, the PDF of stretching factors $P(\rho)$ becomes more and more peaked as time evolves, since the variance $\langle(\log\rho - \langle\log\rho\rangle)^2\rangle^{1/2}$ increases slower (as $\sqrt{t}$) than the mean stretching factor $\langle\log\rho\rangle$ (which increases as t). The spectrum should thus tend

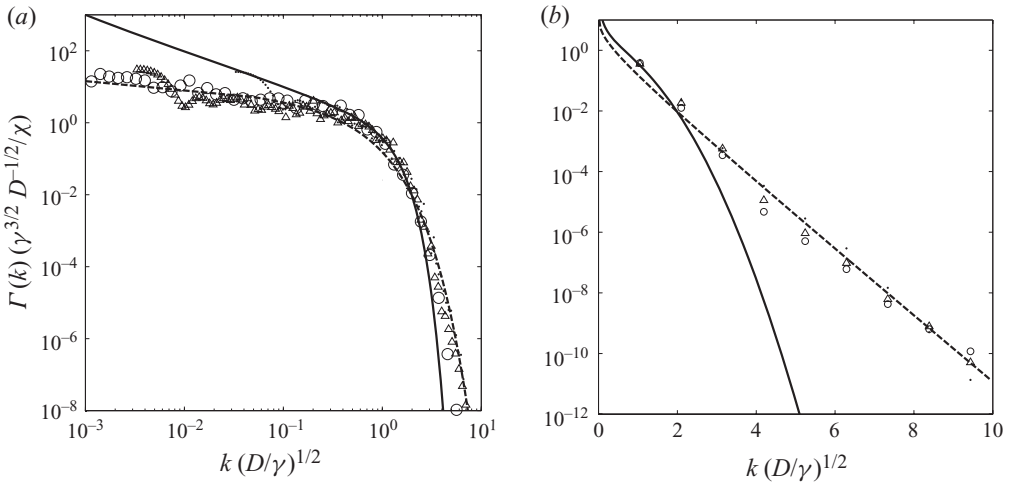

FIGURE 13. Energy spectrum of the scalar at $t=7$ obtained by direct integration along the strip. The Péclet number is equal to $Pe=10^3$ (•), $Pe=10^5$ (△) and $Pe=10^7$ (○). The solid line corresponds to the Batchelor spectrum (5.5) and the dashed line corresponds to the solution (5.9) proposed by Kalda (2000) for decaying turbulence. The scale for the wavenumber is (*a*) logarithmic and (*b*) linear.

towards the Batchelor spectrum at late stages (with a cutoff as e^{-k^2}). However, even if a strip is stretched by a factor ρ over a period t, this does not imply that the stretching rate has been constant and equal to $\gamma=(\log\rho)/t$. The variation of the stretching rate with time induces a variation of the Batchelor scale $\sqrt{D/\gamma}$, which broadens the final spectrum although the stretching factors (integrated over time) are all equal.

5.3. *Spectrum of a decaying scalar*

We now turn to the case of the energy spectrum of the scalar when the strip is injected at $t=0$ only, as was described in § 3. The strip is not injected at each period as it was in § 5.2, such that this is now a decaying field. Figure 13 shows the spectrum of the scalar field at $t=7$ for three different Péclet numbers. It is clear that the numerical results are below the Batchelor spectrum (5.5) at low wavenumbers. This comes from the fact that the energy present at small wavenumbers at $t=0$ has moved towards the large wavenumbers, thus creating a defect of energy at low wavenumbers since there is no injection of energy there. The disagreement is especially visible at high Péclet number ($Pe=10^7$) since the spectrum is resolved on three decades in k.

For a decaying scalar, the differential equation (5.7) is still valid, but we do not look for a stationary solution with a boundary condition at $k=0$. We instead look for a decaying solution with an initial condition at $k\Gamma(k,t=0)=\delta(\log k)$, meaning that all the energy is in the initial length scale ($k=1$) at $t=0$. Kalda (2000) showed that the solution tends towards a Hankel function of order zero at late stages

$$\Gamma(k)=\mathrm{i}e^{-\gamma t/3}H_0^{(1)}\left(\mathrm{i}k\sqrt{6D/\gamma}\right). \tag{5.9}$$

This solution is plotted as a dashed line in figure 13 and is in fairly good agreement with the numerical result at low wavenumbers. This solution is not a pure power law at low wavenumbers. Figure 13(*b*) shows that the solution is in excellent agreement with the numerical results at high wavenumbers, with an exponential decay e^{-k} as in the Kraichnan model, due to distributed stretching rates. To conclude, the model

for the stretching rate allows prediction of the energy spectra of the scalar through a differential equation which is directly connected to the differential equation of the PDF of stretching factors. The solutions do not contain any fitting parameter and are in excellent agreement with the numerical results on four decades in k. The simulation clearly makes the distinction between a stationary, and a decaying scalar field on their respective spectral signature.

6. Probability distribution function of the scalar

6.1. *Two methods to calculate the PDF*

An important question in scalar mixing is to provide a description of the concentration content $P(c)$ of the mixture. $P(c)\,\mathrm{d}c$ is defined as the normalized number of pixels (in the simulation, otherwise, regions of space) whose concentration is in the interval $[c,\ c+\mathrm{d}c]$. Numerically, it can be computed by calculating the histogram of the scalar spatial distribution $c(\boldsymbol{x})$ and renormalizing it such that $\int P(c)\,\mathrm{d}c = 1$. For the same reason as in § 5 for the spectrum, this method is tedious since it needs a reconstruction of the scalar distribution (very demanding in memory because c is a two-dimensional matrix).

However, there is, as for the spectrum, an alternative way to compute the PDF $P(c)$. Using the fact that the strip has a Gaussian profile defined by (2.8), each segment $[\boldsymbol{x}_i\ \boldsymbol{x}_{i+1}]$ has a histogram of concentration given by

$$N_{[\boldsymbol{x}_i\ \boldsymbol{x}_{i+1}]}(c) = \frac{s_i \Delta l}{c} \sqrt{\frac{1+4\tau_i}{-\log(\sqrt{1+4\tau_i}\ c/c_0)}}, \tag{6.1}$$

where Δl is the length of the interval $[\boldsymbol{x}_i\ \boldsymbol{x}_{i+1}]$. In our simulations, the set of tracers $\boldsymbol{x}_i$ is reinterpolated before computing the PDF, such that the tracers are equally spaced (see § 2). This histogram has a well known U-shape, with a divergence as $1/c$ at low concentrations and a logarithmic divergence at the maximal concentration $c_0/\sqrt{1+4\tau_i}$. It comes from the large number of pixels with $c=0$ (far from the strip), and the large number of pixels close to the maximum of the Gaussian at the maximal concentration (at the centre of the strip, i.e. at $n=0$). A major problem of this histogram is that it cannot be renormalized since $\int P(c)\,\mathrm{d}c$ diverges because of the divergence in $c=0$. This property comes from the fact that a Gaussian profile extends on an infinite domain. It is intrinsic to the diffusion equation, which is in fact an ill-posed problem in an infinite domain. The consequence is that the PDFs are defined with a normalizing constant which cannot be calculated analytically.

The total PDF is obtained as the sum of the histograms of each segment $P(c) = A \sum_i N_{[\boldsymbol{x}_i\ \boldsymbol{x}_{i+1}]}(c)$ if the different intervals do not interfere with each other (A being a normalizing constant). This is the case at large Péclet number and/or at early stages (see § 3). However, unlike the calculation of the spectrum, this method becomes invalid if there is some overlap between different parts of the strip, because the PDF is a nonlinear function of the concentration c. But, it is still interesting to use this method and to compare its result to the exact PDF, since it precisely quantifies the amount of self-overlap of the strip.

6.2. *PDF of a solitary strip*

Figure 14 shows the PDF of concentration for a strip advected by the sine flow presented in § 3. The PDF is plotted at $t=7$, which corresponds to the scalar

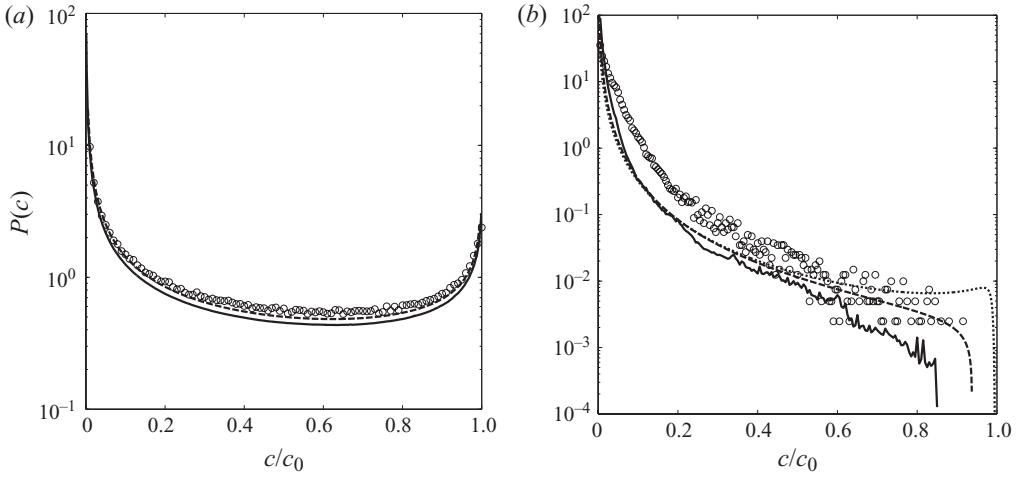

FIGURE 14. PDF of the scalar distribution for a strip in a sine flow at $t = 7$ as in figure 7(d). The Péclet number is equal to $Pe = 10^{10}$ (a) and $Pe = 10^5$ (b). The true PDF (○) is computed by doing a histogram of the spatial distribution of scalar. Solid lines correspond to an approximate PDF, computed by doing an integration of the Gaussian profile along the strip using (6.1). Dashed lines correspond to the prediction (6.3) using the log-normal model of stretching. Dotted line is the PDF of maximal concentration given by (6.4) for the log-normal model of stretching.

distribution shown in figure 8. At high Péclet number ($Pe = 10^{10}$), the strip has not yet reached the mixing time so that the maximal concentration is almost everywhere equal to the initial concentration c_0. The logarithmic divergence of each interval's histogram is located at $c = c_0$. The total PDF is thus a U-shaped PDF between $c = 0$ and $c = c_0$. It can be recovered easily by assuming $\tau_i \ll 1$ in (6.1), leading to a PDF proportional to $1/c\sqrt{-\log(c/c_0)}$ (see also Meunier & Villermaux 2003). There is a good agreement between the two methods used to calculate the PDF since there is no aggregation at this high Péclet number (as visible in the inset of figure 8b).

At moderate Péclet number ($Pe = 10^5$), the strip has started to diffuse, filling the low levels of concentrations in the PDF. The logarithmic divergence disappears, because there is no point on the strip where the maximal concentration is equal to c_0. The PDF becomes a decreasing function of c, with an inverted S-shape characteristic of flows with a broad distribution of stretchings (Duplat, Innocenti & Villermaux 2010). There is, moreover, a slight discrepancy between the two methods used to compute the PDF. This means that some aggregation of the strip with itself has occurred. The exact PDF (plotted as symbols) is slightly above the ideal PDF that would be obtained if the strip was not overlapping with itself (plotted as a solid line).

In order to understand these PDFs, we use the model of multiple step stretching, which leads to a log-normal law (4.14) for the PDF of stretching factors. The strip can thus be modelled as a sum of segments of length $P(\rho)\,\mathrm{d}\rho$, which have been stretched by a factor ρ in a time t. For a stretching rate assumed constant in time (equal to $\log(\rho)/t$), the striation thickness decreases exponentially in time and the dimensional time τ can be calculated by integration of (2.6) as

$$\tau(\rho) = \frac{Dt}{2s_0^2}\,\frac{\rho^2 - 1}{\log\rho}. \tag{6.2}$$

Equation (6.1) then leads to an analytical formula for the PDF of concentration, if Δl is replaced by $P(\rho)\,\mathrm{d}\rho$ and s by s_0/ρ:

$$P(c) = \frac{A}{c}\int_{\tau(\rho)<((c_0^2/4c^2)-(1/4))} \sqrt{\frac{1+4\tau(\rho)}{-\log(\sqrt{1+4\tau(\rho)}\,c/c_0)}}\,\mathrm{e}^{-((\log\rho-2\gamma t/3)^2)/(4\gamma t/3)}\,\frac{\mathrm{d}\rho}{\rho}, \quad (6.3)$$

where A is a normalizing constant, and the mean stretching rate γ has been calculated numerically for the sine flow ($\gamma = 0.91$).

This solution is plotted in figure 14 as a dashed line. It is in very good agreement with the numerical results at high Péclet number ($Pe = 10^{10}$). This is not a surprise because the dimensionless time τ is much smaller than one for the stretching factors which have a high probability $P(\rho)$, such that the integral in (6.3) simplifies into $1/\sqrt{-\log(c/c_0)}$, leading to a U-shaped PDF.

For a moderate Péclet number ($Pe = 10^5$), the theoretical prediction is still in fairly good agreement with the PDF obtained if there was no aggregation of the strip (plotted as a solid line), especially at low concentrations. For such a moderate Péclet number (where the mixing time has been reached everywhere), it is common to calculate the PDF of maximal concentration $Q(c)$, which is obtained by assuming that the strip has a square profile of width $s\sqrt{1+4\tau}$ instead of a Gaussian profile. The PDF is then defined by $Q(c)\,\mathrm{d}c = s\sqrt{1+4\tau(\rho)}P(\rho)\,\mathrm{d}\rho$ which gives an analytical expression for the PDF:

$$Q(c) \sim \frac{P(\rho)\log(\rho)^2}{c^4(1-\rho^2+2\rho^2\log\rho)} \quad \text{with} \quad \rho = \tau^{-1}\left[\frac{c_0^2-c^2}{4c^2}\right]. \quad (6.4)$$

Here, τ^{-1} is the inverse function of $\tau(\rho)$ defined in (6.2). This solution is plotted in figure 14(b) as a dotted line. It is in fair agreement with the previous theoretical PDF at low concentrations, because the PDF is there a decreasing function of c. However, there is a small deviation at high concentrations. This reasoning would not work at high Péclet number ($Pe = 10^{10}$) because the PDF $Q(c)$ is then the sum of two Dirac functions at $c = 0$ and $c = c_0$, whereas the exact PDF is U-shaped, corresponding to a Gaussian profile.

6.3. *PDF of a strip with reconnection*

We have seen in § 5 that the PDF calculated by integrating along the strip the histogram of a Gaussian profile (6.1) is not equal to the exact PDF (calculated directly as a histogram of the scalar distribution) at late stages, and at moderate Péclet numbers. This originates from the aggregation of different parts of the strip, which occurs when the thickness of the strip (in the presence of diffusion) becomes of the order of the distance between two adjacent elements of the folded strips. To understand better how these reconnections modify the PDF, we have increased the number of reconnections by placing initially several long strips in the sine flow instead of a single-short strip. This can be done very easily (without further computation) if the strips are along the x-axis and infinite at $t = 0$. Indeed, if the computation was done for a strip $\boldsymbol{x}_i$ initially located between $x = -0.5$ and $x = 0.5$, an initially infinite strip is obtained as the sum of strips located in ..., $(x_i - 3, y_i)$, $(x_i - 2, y_i)$, $(x_i - 1, y_i)$, (x_i, y_i), $(x_i + 1, y_i)$, $(x_i + 2, y_i)$, $(x_i + 3, y_i)$, ... because the sine flow is periodic with a wavelength equal to 1 in the x-direction. The same argument can be used in the y-direction: an initial column of strips separated by one in the y-direction is obtained as a sum of strips located in ..., $(x_i, y_i - 3)$, $(x_i, y_i - 2)$, $(x_i, y_i - 1)$, (x_i, y_i), $(x_i, y_i + 1)$,

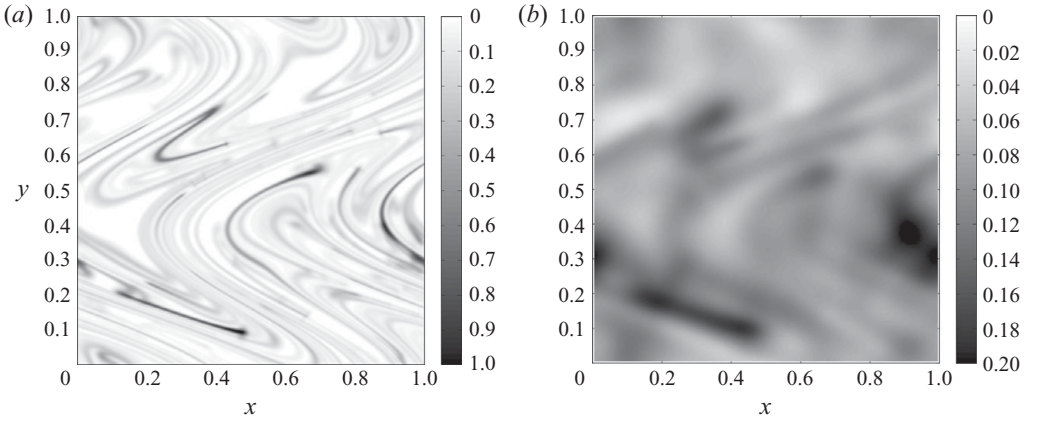

FIGURE 15. Spatial distribution of a strip of scalar in a sine flow at $t = 7$ for a Péclet number equal to (*a*) 10^5 and (*b*) 10^3. All points of the strip have been translated into the unit square in order to model a periodic initial condition (and flow) composed of a column of strips infinite in x and located at $y = \ldots, -2, -1, 0, 1, 2, \ldots$

$(x_i, y_i - 2)$, $(x_i, y_i + 3)$, ... because the sine flow is periodic in the y-direction with a wavelength equal to 1.

The distribution of scalar obtained for such an initial condition is plotted in figure 15 for various Péclet numbers. It is only plotted for $0 < x < 1$ and $0 < y < 1$ because the distribution is periodic. While the strips are still discernible for $Pe = 10^5$, the field is almost homogeneous for the lowest Péclet number ($Pe = 10^3$). The density of strips is so large that the mean distance between two strips is smaller than their mean width.

The PDFs of concentration corresponding to these scalar fields are plotted in figure 16 as symbols. For $Pe = 10^5$, the PDF is decreasing at large concentrations but it presents a plateau with a small maximum at $c = 0.1c_0$. For $Pe = 10^3$, this maximum is clearly visible, which corresponds to the fact that the field tends to be homogeneous with a mean concentration equal to the total quantity of scalar $\int c_0 L_0 \mathrm{e}^{-n^2/s_0^2}\,\mathrm{d}n$ divided by the area of the periodic domain (here, $\langle c \rangle = \sqrt{\pi} s_0 c_0 = 0.0886 c_0$).

These PDFs are very different from those obtained by assuming that the strip has evolved on its own, independently of its neighbours (calculated in (6.1)), which are plotted as black solid lines. This strong difference is not surprising, since the PDF is a highly nonlinear function of c, while the concentration levels of overlapping strips interact in an additive fashion, owing to the linearity of the Fourier equation (Villermaux & Duplat 2003). Precisely, if two strips with concentrations c_1 and c_2 such that $c = c_1 + c_2$ overlap, the total scalar field c has a PDF given by

$$P(c) = \int_{c=c_1+c_2} P_1(c_1) P_2(c_2)\,\mathrm{d}c_2, \tag{6.5}$$

where $P_1(c_1)$ is the PDF of the first strip and $P_2(c_2)$ that of the second. If the concentration levels c_1 and c_2 in (6.5) are chosen at random among those available in the original distributions P_1 and P_2, with no particular correlation or constraint, then (6.5) defines a convolution of the original distributions. The consequence of this interaction rule on the structure of $P(c)$ itself has been discussed for several random flows (Villermaux & Duplat 2003; Duplat & Villermaux 2008; Villermaux, Stroock & Stone 2008), leading to a family of distributions stable by self-convolution.

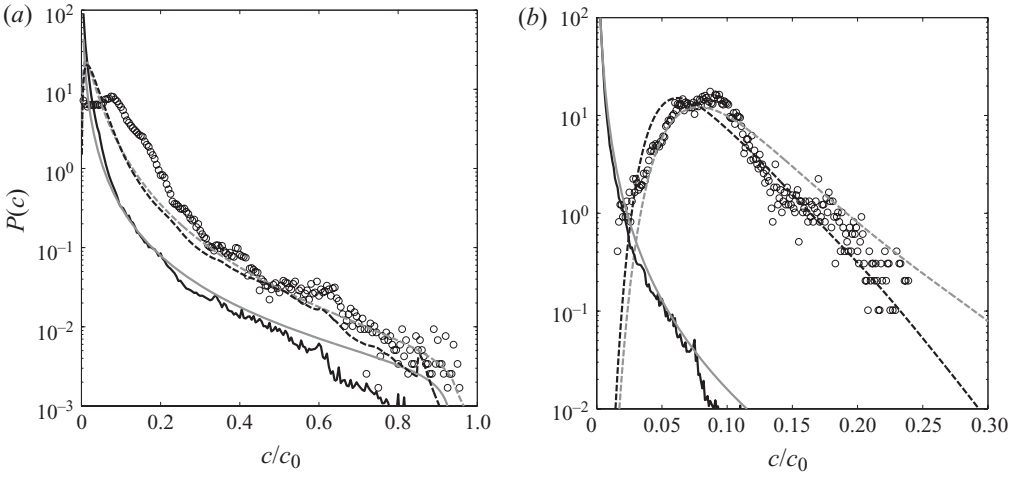

FIGURE 16. PDF of the scalar distribution for a strip in a sine flow at $t = 7$, where the flow has been made periodic as in figure 15. The Péclet number is equal to $Pe = 10^5$ (*a*) and $Pe = 10^3$ (*b*). Symbols are calculated by doing a histogram of the spatial distribution of scalar. Black solid lines are calculated by doing an integration of the Gaussian profile along the strip using (6.1). Grey solid lines correspond to the prediction (6.3) obtained using the log-normal model of stretching. The dashed lines are computed by self-convolving N times the solid lines, with (*a*) $N = 4$ and (*b*) $N = 43$, as predicted by (6.6).

The present simulations offer a unique way of testing the relevance of this interaction rule: in the case of a single strip which aggregates with itself, the PDF in the presence of aggregation should be obtained as the convolution of the PDF without aggregation, which we know from the solitary PDF $P_{single}(c)$ discussed in § 6.2. If the strip reconnects several times with itself, the PDF must be convolved as many times. Let us call this number of convolutions N, we thus expect

$$P(c) = P_{single}(c)^{\otimes N}. \tag{6.6}$$

The result of this convolution is plotted in figure 16 as dashed lines and compared to the true PDF characterizing the true field (plotted as symbols). The agreement is fair for $Pe = 10^5$ and it is very good for $Pe = 10^3$: the self-convolved PDF indeed presents a plateau around $c = 0.1c_0$ and the width of the peak is well predicted. This actually means that the aggregation of the strip with itself is indeed the process by which the complex mixture has been built, and is well described by a self-convolution of the solitary PDF with itself.

The number of convolutions N needed to adjust the self-convolved solitary PDF onto the exact PDF is plotted in figure 17(*a*). It has been calculated in two different ways by taking either the theoretical prediction (6.3) for the PDF of the solitary strip, corresponding to the grey lines of figure 16 or by taking for the solitary strip the PDF obtained numerically by integration of (6.1), corresponding to the black lines of figure 16. The number of convolutions N increases exponentially with an exponent very close to $2\gamma/3$. This is surprising because the total length of the strip (and thus its surface) increases as $e^{\gamma t}$ and one could have expected the number of convolutions to be proportional to the surface of the strip, leading to an exponent γ and not $2\gamma/3$. These simulations reveal that the number of convolutions is governed by the most probable stretching rate $2\gamma/3$ and not by the mean stretching rate γ.

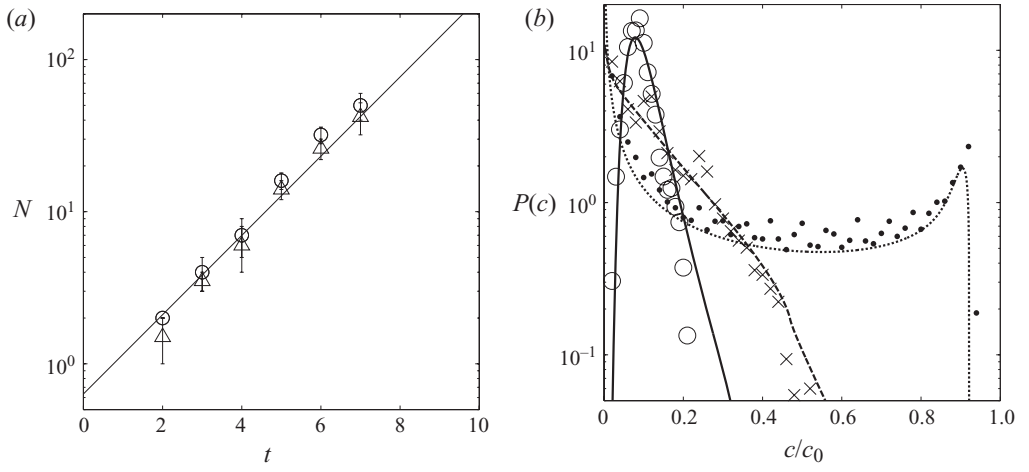

FIGURE 17. (*a*) Temporal evolution of the number of self-convolutions N needed to transform the PDF of a solitary strip (i.e. in the absence of reconnection) into the exact PDF (with reconnections) obtained numerically by doing a histogram of the spatial distribution of scalar. The PDF of the solitary strip is either (○) calculated numerically by integrating (6.1) along the strip or (▽) given by the theoretical prediction (6.3). The solid line corresponds to the theoretical prediction (6.7) for the number of convolutions. (*b*) PDF of scalar obtained for $Pe = 10^3$ at $t = 0.1$ (dotted line, •), at $t = 2$ (dashed line, ×) and at $t = 7$ (solid line, ○). Symbols correspond to the exact numerical result. Lines correspond to the PDF given by (6.3) and self-convolved N times with N given by (6.7).

This number of convolutions can be calculated in the simplified case where all strips are subject to the same stretching rate $\gamma_p = 2\gamma/3$. In this situation, all strips have a Gaussian normal profile $c(n) \sim \mathrm{e}^{-\gamma_p n^2/2D}$. By definition, two strips reconnect if their levels are larger than a minimum level dc on a common area, which is achieved if their distance is smaller than a minimum distance $\Delta = 2\sqrt{-2D \log dc/\gamma}$ for Gaussian profiles. Since the mean distance between two strips decreases as $d_0\mathrm{e}^{-\gamma_p t}$ (d_0 being the initial mean distance between two strips), each strip reconnects with a number of strips equal to

$$N = \frac{2\Delta}{d_0\mathrm{e}^{-\gamma_p t}} = \frac{4}{d_0}\sqrt{-\frac{3D}{\gamma}\log(dc)}\,\mathrm{e}^{2\gamma t/3}. \tag{6.7}$$

In our simulations, d_0 is equal to 1 in the periodic case and dc is a numerical constant for the scalar step, which is taken equal to 5×10^{-4}. It can be noted that this analytical formula diverges when dc tends to 0, but this divergence is very slow (scaling as $\log(dc)^{1/2}$, which makes it very weakly dependent on this numerical constant. This is in fact a consequence of the fact that a Gaussian profile extends to infinity and has thus a non-normalized PDF. This prediction is plotted in figure 17(*a*) as a solid line and is in excellent agreement with the empirical determination of the number of convolutions.

To conclude, it is possible to use the theoretical prediction of the PDF (6.3) in the absence of aggregation and to convolve it N times according to (6.7), giving a prediction for the PDF expected in the presence of aggregation. These PDFs are plotted in figure 17(*b*) at various times. It predicts correctly the shape of the PDF in the three different regimes: a U-shaped PDF at early stages, a decreasing PDF at intermediate times and a peaked PDF at late stages. The agreement is also

quantitatively correct although it is not perfect. It should be noted, however, that this analytical solution does not contain any fitting parameter, since the mean stretching rate γ is known. It bridges a microscopic description of diffusion on a stretched substrate with a global quantity such as the scalar PDF in a non-trivial flow, from first principles.

6.4. *Why does the convolution rule work so well?*

An interesting question to ask is why the convolution rule, which assumes the absence of correlation between the concentration levels adding at random, works so well. A possible justification is as follows: we have shown in § 5 that the sine flow, like all smooth random flows, has a spatial concentration field $c(\boldsymbol{x})$ with a $\Gamma(k) \sim k^{-1}$ spectrum. This means that the correlation function of the field $\langle c(\boldsymbol{x})c(\boldsymbol{x}+\boldsymbol{r})\rangle_x$ is equal to a constant $\langle c^2\rangle$ minus a rapidly varying function of r scaling as $\log(\gamma r^2/D)$, the inverse Fourier transform of k^{-1}, making the correlation function essentially zero for $r \gg \sqrt{D/\gamma}$. Distant concentration levels are thus very weakly correlated. The role of the large scale advection of the flow is to bring close to each other (i.e. at distances smaller than $\sqrt{D/\gamma}$) these distant concentration levels, which there merge under the blurring action of diffusion, defining a new concentration level equal to their sum. But since these concentration levels were basically uncorrelated, their addition is made at random, with a probability equal to the product of their respective probability of occurrence in the current distribution $P(c)$. The proper interaction rule is thus indeed of a pure convolution type, expressing an effective maximal randomness in the flow. We will have a confirmation of this fact in § 7.

6.5. *Variance of the scalar*

A traditional way since Corrsin (1952) and Danckwerts (1952) of characterizing the progress of a mixture towards uniformity, is to concentrate on the second moment of the PDF, namely the variance of the scalar $\langle c^2\rangle$ (also called intensity of segregation), which can be derived from the knowledge of the PDF $P(c)$. In a confined mixture with conserved average concentration $\langle c\rangle$, the variance decays and relaxes towards $\langle c\rangle^2$ at late stages. The decay is prescribed by that of the maximal concentration in the strips, and is therefore exponential in time after the mixing time.

We have computed the scalar variance for the sine flow directly using the diffusive strip method by reconstructing the scalar field on the domain $-2 < x < 2$ and $-2.5 < y < 2.5$ (with an area $\mathscr{A} = 20$), where the scalar is initially introduced for $-0.5 < x < 0.5$ as in § 3. The variance is plotted in figure 18 as a function of time for two different Péclet numbers. It is indeed decaying exponentially after $t = 2$. The variance is smaller for smaller Péclet numbers, for which the mixing time is smaller. The late evolution is nevertheless independent in law of the Péclet number (i.e. exponential with the same decay rate).

It is fairly easy to give an analytical solution for the variance for a solitary strip. Indeed, the log-normal model for the strip stretching indicates that the length of the strip which has been stretched by a factor ρ is equal to $P(\rho, t)L(t)$ where $L(t) = L_0 \mathrm{e}^{\gamma t}$ is the total length of the strip and $P(\rho, t)$ is given by (4.14). For a given stretching factor ρ, the transverse profile is Gaussian with a parameter $s_0\sqrt{1+4\tau}/\rho$ and a maximal concentration equal to $c_0/\sqrt{1+4\tau}$, where the dimensionless time τ is given by (6.2). This leads to an integral of the squared concentration profile in its transverse direction as

$$\int_{-\infty}^{+\infty} c^2(n)\,\mathrm{d}n = \frac{c_0^2 s_0\sqrt{\pi/2}}{\rho\sqrt{1+4\tau}}. \tag{6.8}$$

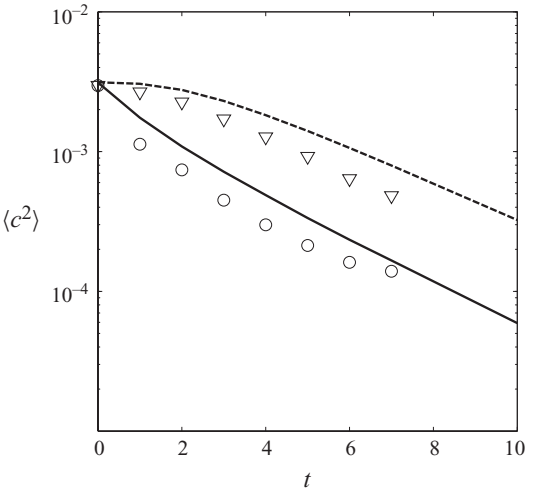

FIGURE 18. Variance of the field of scalar as function of time for $Pe = 10^3$ ($\circ$) and $Pe = 10^5$ ($\triangledown$). Lines correspond to the theoretical prediction of (6.9).

The variance is then obtained as the sum along the strip of this integral multiplied by the length $P(\rho, t)L(t)\,\mathrm{d}\rho$ and divided by the total area $\mathscr{A}$ of the domain

$$\langle c^2 \rangle = \frac{c_0^2 L_0 s_0}{\mathscr{A}\sqrt{8\gamma t/3}} \int_0^{+\infty} \exp\left[-\frac{(\log\rho - 2\gamma t/3)^2}{4\gamma t/3}\right] \frac{\mathrm{d}\rho}{\rho\sqrt{1+4\tau(\rho)}}. \tag{6.9}$$

This prediction is plotted in figure 18 for two different Péclet numbers. It overestimates the numerical result, which may come from the aggregation of the strip with itself. However, the theory recovers an exponential decay at late stages, with a correct decay rate. An asymptotic formula can be obtained for $\tau \gg 1$ by cutting the integral at $\log\rho = (\gamma t)^{1/4}$ showing that at late stages the variance tends to

$$\langle c^2 \rangle = \frac{c_0^2 L_0 s_0^2 \mathrm{e}^{-\gamma t/3}}{2\mathscr{A}\sqrt{D}} \left(\frac{\gamma}{6t}\right)^{1/4} \int_0^{+\infty} \sqrt{x}\,\mathrm{e}^{-x^2/2}\,\mathrm{d}x, \tag{6.10}$$

with $\int \sqrt{x}\,\mathrm{e}^{-x^2/2}\,\mathrm{d}x = 1.0304$. At leading order, the variance thus decays exponentially with time, as seen in figure 18 with a decay rate $\gamma/3$ indeed correctly predicted.

It is curious to see that the variance, the number of convolutions N and the total length L of the strip, if they all behave exponentially in time, have three different exponents. This is a consequence of the log-normal law $P(\rho)$ which is very broad and contains large and small stretching factors ρ at the same time. The total length of the strip is more sensitive to large stretching factors since they create proportionally a larger interval on the final strip. The total length thus increases with a rate γ which is larger than the most probable stretching rate $2\gamma/3$. On the contrary, the variance is more sensitive to the least elongated parts of the strip, since they bear higher levels of concentration. The variance thus decreases with a rate $\gamma/3$ smaller than the most probable stretching rate. The number of convolutions N is sensitive to both concentration levels and length of the strip, and increases at the most probable stretching rate.

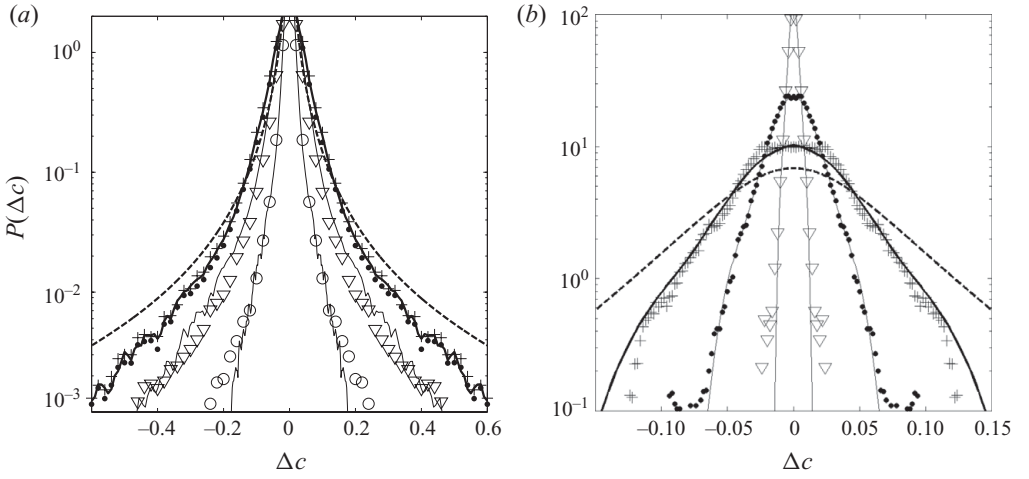

FIGURE 19. PDF of increments of scalar Δc for a strip in a sine flow at $t = 7$. (*a*) The Péclet number is equal to $Pe = 10^5$ and the scalar is initially injected between $-0.5 < x < 0.5$, which leads to the distribution of scalar of figure 7(*d*). (*b*) The Péclet number is equal to $Pe = 10^3$ and the scalar is initially periodic in both x- and y-direction, which leads to the distribution of scalar of figure 15(*b*). The increment Δc is taken between two points separated by $\Delta x = 0.003$ ($\circ$), $\Delta x = 0.01$ ($\triangledown$), $\Delta x = 0.05$ ($\bullet$) and $\Delta x = 0.2$ ($+$). Thick solid lines are obtained as the convolution $P(c) * P(-c)$ of the numerical PDF of scalar with its symmetric part. Thin solid lines are deduced from this PDF by a dilatation with a factor $\Delta x/\eta$ where the Batchelor scale η is equal to 0.014 in (*a*) and 0.12 in (*b*). Dashed lines correspond to the convolution $P(c) * P(-c)$ of the theoretical PDF of scalar given by (6.3) and convolved with itself N times with N given by (6.7): in (*a*) $N = 1$ and in (*b*) $N = 48$.

7. Probability distribution function of scalar increments

As a complement, it is useful to study the PDF of scalar increments because it gives further insights into the spatial structure of the scalar distribution, and also because it legitimates the use of the maximal randomness property made in § 6.3.

We define the PDF of the increment $\Delta c = c(\boldsymbol{x}) - c(\boldsymbol{x} + \Delta x\, \boldsymbol{e})$ of scalar concentration between two points separated by a distance Δx ($\boldsymbol{e}$ being a unit vector which has been taken along x and along y in the simulations). These PDFs are plotted in figure 19 for two different Péclet numbers and aggregation conditions. In figure 19(*a*), the initial scalar distribution is a unique strip and the Péclet number is relatively high ($Pe = 10^5$) such that there is basically no aggregation of the strip with itself at $t = 7$. In figure 19(*b*), on the contrary, the scalar is injected initially as a dense periodic pattern and the Péclet number is smaller $Pe = 10^3$ so that reconnections of the strip with itself are more frequent.

In the case of a solitary strip (no aggregation), the PDF of increments is extremely peaked around zero and has strong non-Gaussian tails. These large increments correspond to the high values of scalar located on the unmixed regions of the strip. When the distance Δx increases, the PDF gets wider up to a certain distance $\eta = 0.014$ above which it remains invariant whatever the value of Δx. This is a direct proof that above this distance, the concentrations $c(\boldsymbol{x})$ and $c(\boldsymbol{x} + \Delta x)$ are uncorrelated. Indeed, in this large Δx limit, the probability of having an increment Δc can be calculated as the probability $P(c_1)$ that the concentration equals c_1 in $\boldsymbol{x}$ multiplied by the probability $P(c_2)$ that the concentration equals c_2 in $\boldsymbol{x} + \Delta x$, with $c_1 + c_2 = \Delta c$. When summing over c_2 and assuming that the probabilities are independent, one gets that the PDF

of increments $P(\Delta c)$ is equal to the convolution product of the PDF of scalar $P(c)$ with $P(-c)$

$$P_{\Delta x}(\Delta c) = P(c) \otimes P(-c), \quad \text{for} \quad \Delta x > \eta. \tag{7.1}$$

This solution is plotted as a thick solid line in figure 19(a), where the PDF of concentration $P(c)$ is given by the numerical simulation (the corresponding symbols are those of figure 14b). There is an excellent agreement with the PDF of increments for Δx larger than $\eta = 0.014$, an agreement even better than the one achieved using for the field PDF $P(c)$ obtained in (6.3) convoluted N times and transformed according to (7.1).

For small distances Δx, the PDF of increments becomes narrower. This is easily understood by the fact that the concentration $c(\boldsymbol{x})$ is now correlated with the concentration $c(\boldsymbol{x} + \Delta x)$ since now Δx explores the internal structure of the strip or of a bundle of strips in the process of merging. An easy way to calculate the PDF of increment is then to assume that all the strips have the same thickness η. For $\Delta x < \eta$, the increment Δc is then proportional to Δx (assuming that a triangle is a good representation of the strip transverse concentration profile), and the PDF of increment is squeezed by a factor $\Delta x/\eta$

$$P_{\Delta x<\eta}(\Delta c) = \frac{\eta}{\Delta x} P_{\Delta x>\eta}\left(\frac{\eta}{\Delta x}\ \Delta c\right). \tag{7.2}$$

This prediction is plotted as thin solid lines in figure 19(a) with $\eta = 0.014$, and shows a good agreement with the numerical values of the PDF of increments.

In the case of a strip with many aggregations (as in figure 19b), the PDF is closer to Gaussian at its centre, but still presents substantial wings at large increments Δc. As in the case of the solitary strip, it gets wider when the distance Δx increases, but it now saturates at a larger value equal to $\eta = 0.12$ (the Péclet number is lower). As previously discussed, this means that for large distances $\Delta x > \eta$, the concentrations $c(\boldsymbol{x})$ and $c(\boldsymbol{x} + \Delta x)$ are uncorrelated and the PDF is given by (7.1) as the convolution of $P(c)$ and $P(-c)$. This prediction is plotted as a thick solid line in figure 19(b), where $P(c)$ is determined numerically (the corresponding symbols are those of figure 16b). There is an excellent agreement with the numerical result of $P(\Delta c)$. However, the same remark applies as for the solitary strip: the theoretical prediction of $P(c)$ given by (6.3) convolved N times and transformed according to (7.1), plotted as a thick dashed line, leads to a less good agreement.

For small distances $\Delta x < \eta$, the PDF of increment is again found by squeezing the PDF of increment at large distances by a factor $\Delta x/\eta$, as defined by (7.2). This prediction is plotted in figure 19(b) by thin solid lines and presents an excellent agreement with the numerical results.

We have seen that the PDF of increment can be predicted using (7.1) for large distances ($\Delta x > \eta$) and using (7.2) for small distances ($\Delta x < \eta$). The question thus remains to determine what controls this critical distance η. It reflects the distance over which $c(\boldsymbol{x})$ correlates with itself. It thus scales as the distance over which diffusion has blurred the concentration differences. That distance is larger than the Batchelor scale $\sqrt{D/\gamma}$ itself since a bundle of elementary strips (whose width is $\sqrt{D/\gamma}$) in the process of aggregating realizes a smooth ensemble at the scale of the bundle itself. This coarse-grained scale is thus larger than the typical size of the concentration gradient in the flow (larger than the spectrum diffusive cutoff) and has been found to decreases like $Pe^{-1/2}$ as well in exponential flows, like the sine flow (Villermaux & Duplat 2006). Figure 19 shows that $\eta \approx 4\sqrt{D/\gamma}$ in the present flow.

8. Conclusion

We have introduced a new numerical method for the study of scalar mixing in two-dimensional advection fields. This method is inspired by the empirical observation that natural flows tend to form elongated structures, making a mixture a collection of adjacent strips (sheets in three dimensions), more or less diffuse and overlapping.

As explained in § 2, the position of an advected material strip is computed kinematically, and the associated convection–diffusion problem is solved using the computed local stretching rate along the strip, assuming that the diffusing strip thickness is smaller than its local radius of curvature. This assumption, which is legitimate at high Péclet number, reduces the numerical problem to the computation of a single variable along the strip, thus making the method extremely fast and applicable to any large Péclet number. Since it is grounded on the use of a near-exact solution of the Fourier equation, this method is also extremely precise. This new numerical method makes the link between the spectral methods which are limited to small Péclet numbers and the standard Lagrangian tracking methods which do not model the diffusion of a scalar, but only study its stirring by the flow. This strip diffusion method is thus the only numerical method able to solve the advection–diffusion problem in the cases of large Péclet numbers. However, it is not suitable for small Péclet numbers, and it also exhibits some numerical artefacts localized in cusps.

This method is the analogue of the contour dynamics method which has been introduced 30 years ago to solve the Euler equation in two dimensions (Zabusky, Hughes & Roberts 1979) and which is widely used now. Indeed, it uses a reduction of the two-dimensional field to a one-dimensional contour, which greatly decreases the amount of data needed to describe the whole field. The advantage is that the problem can be solved by a computer with a limited memory and also that it is much faster than the standard spectral methods. We thus expect this method to be of interest in the field of turbulent mixing.

As a first step, we have used this method to document the mixing properties of a chaotic sine flow (§§ 3–7), for which we have related the global quantities (spectra, concentration PDFs, increments) to the distributed stretching of the strip convoluted by the flow, possibly overlapping with itself. The numerical results indicate that the PDF of the strip elongation is log-normal, a signature of random multiplicative processes. This property lead to exact analytical predictions for the spectrum of the field and for the PDF of the scalar concentration of a solitary strip, in good agreement with the numerical results. A further analogy with stochastic processes for which the deterministic part of the stretching has the same weight as the noise has further reduced the description of the flow to a unique parameter, namely the mean stretching rate γ (see § 4.4).

The present simulations, since they keep track of both the contribution of a solitary strip, and of the global concentration PDF (as opposed to presently available experiments where these two pieces of information are mingled) offer a unique way of studying the building rules of complex mixtures. The global PDF is simply obtained by convolution of the PDFs of the two reconnecting strips. Interestingly, the number of convolutions needed to restore the full mixture PDF from a solitary strip increases at a rate prescribed by the most probable stretching rate equal to $2\gamma/3$, while the total strip length is stretched at a rate γ. Conversely, the variance decreases as $\mathrm{e}^{-\gamma t/3}$, these differences singling out the broadly distributed character of the stirring field.

A last advantage of the method is also that it can be easily generalized to three-dimensional flows. Indeed, the strip used in this two-dimensional study can be replaced

by a sheet in three dimensions. By calculating numerically the stretching rate of the sheet, it is fairly easy to construct a diffusive time in the same manner and to derive the transverse profile of scalar across the sheet. It thus seems simple to make an extension of this method to three-dimensional flows. However, new numerical problems might arise in the refinement of the sheet and treatment of the cusps.

Another natural extension of this method also would be to consider chemically reacting scalars, in the spirit of the Flamelet models used for turbulent diffusion flames (Peters 1984).

This work has been supported by the Agence Nationale de la Recherche (ANR) through grant ANR-05-BLAN-0222-01. The authors thank J. Duplat for numerous enlightening discussions on scalar mixing.

Appendix. Numerics, computational time and cost

(i) Numerics: In the Matlab code of the strip diffusion method, the equation of motion (1.1) is integrated using an explicit Runge–Kutta (4,5) formula, given by Matlab under the instruction 'ode45'. The time step δt was chosen equal to 10^{-3} for the vortex and a sine flow with a period equal to 1 and a velocity equal to 0.5 (see § 3). Equation (2.6) for the dimensionless time τ is integrated in the most simple manner ($\tau_i(t+\delta t) = \tau_i(t) + \kappa \delta t / s_i(t)^2$), since it proved to be completely converged. Indeed, the striation thickness $s_i(t)$ usually decreases exponentially, making the integration of (2.6) very stable.

(ii) We detail here the technique used to add dynamically tracers on the strip during the calculation, in order to fulfil criterion (2.13). The best method to do so was to calculate numerically the function $F_i = \int_0^{\sigma_i} (1 + \alpha\kappa(\sigma))\,\mathrm{d}\sigma$, where σ_i is the curvilinear abscissa at the tracer $\boldsymbol{x}_i$ (obtained numerically as the cumulative sum of the distance Δx_i between two consecutive points). The new set of tracers $\boldsymbol{x}_j$ were then interpolated such that the corresponding F_j are equally spaced with Δl. In our algorithm, this reinterpolation was done separately on each component of the position $\boldsymbol{x}_i = (x_i, y_i)$, by using a natural cubic spline interpolation provided by Matlab under the instruction csape of the spline toolbox. However, the best results were obtained when the interpolation was made with the position defined as a function of the curvilinear abscissa σ_j instead of F_j ($x_j = \mathrm{interp}(\sigma_i, x_i, \sigma_j)$). The reinterpolated abscissa σ_j were calculated using a basic linear interpolation corresponding to F_j: $\sigma_j = \mathrm{interp}(F_i, \sigma_i, F_j, '\mathrm{linear}')$.

To calculate the curvature κ_i at the tracer $\boldsymbol{x}_i$, the algorithm uses the formula

$$\kappa = \frac{|x'y'' - x''y'|}{(x'^2 + y'^2)^{3/2}}, \tag{A 1}$$

where x' (respectively y') is the derivative of the first (respectively second) component of $\boldsymbol{x}$ with respect to the curvilinear abscissa, which is calculated numerically using the smoothing cubic spline provided by Matlab under the instruction csaps. This allowed calculation of the curvature in a stable way. It may not be exact since it is a smoothing algorithm, but this did not modify the position of the strip but only the density of tracers along the strip. It was also necessary to bound the curvature to 10^5 such that the number of points does not diverge. This criterion did not seem to modify the final position of the strip, even in the regions of the cusps.

During the refinement, the dimensional time τ_i needs also to be reinterpolated into τ_j (corresponding to the refined positions x_j). This was done using a simple

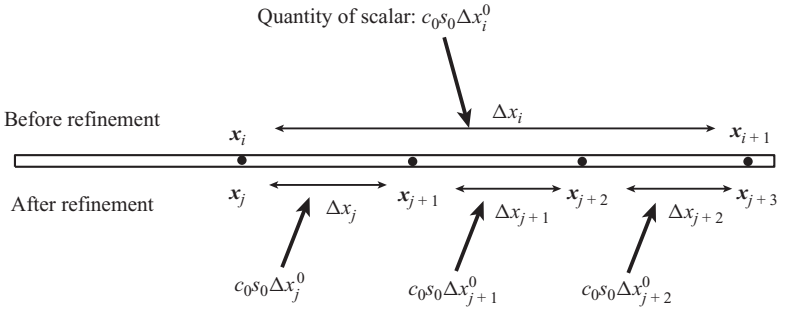

FIGURE 20. Schematic drawing explaining the calculation of the initial separation Δx_i^0 during the refinement. The set of tracers $\boldsymbol{x}_i$ is reinterpolated during the refinement into $\boldsymbol{x}_j$. The quantity of scalar between $\boldsymbol{x}_i$ and $\boldsymbol{x}_{i+1}$ is spread into the three corresponding intervals.

linear interpolation. However, some care had to be taken for the reinterpolation of the striation thickness s_i. Indeed, the striation thickness is linked to the initial length between two tracers Δx_i^0 due to incompressibility. A major constraint is then to respect numerically the conservation of the total quantity of scalar $C = c_0 s_0 \sum \Delta x_i^0$. For this purpose, the algorithm stores the initial length Δx_i^0 between the tracer x_i and the tracer x_{i+1}, instead of the striation thickness s_i since they are related by (2.2). During the refinement from x_i into x_j, the initial length Δx_i^0 is divided into the corresponding intervals Δx_j^0 such that the total quantity of scalar between x_i and x_{i+1} is conserved. In this way, the total quantity of scalar is constant within the numerical accuracy. For example, in the schematic drawing of figure 20, the interval $[x_i\, x_{i+1}]$ is divided into three intervals from x_j to x_{j+3}. The quantity of scalar $c_0 s_0 \Delta x_i^0$ must be equal to $c_0 s_0 \Delta x_j^0 + c_0 s_0 \Delta x_{j+1}^0 + c_0 s_0 \Delta x_{j+2}^0$. Moreover, the intervals Δx_j^0 must be proportional to the Δx_j, which allows the calculation $\Delta x_j^0 = \Delta x_i^0 \Delta x_j / (\Delta x_j + \Delta x_{j+1} + \Delta x_{j+2})$. The algorithm is slightly more complex, because x_j does not correspond in fact to x_i.

The numerical values of Δl and α were chosen depending on the flow, such that the final position of the strip is independent of these constants. For the vortex, a large $\Delta l = 0.05$ was sufficient since the length scale of the vortex is rather large. Moreover, since the vortex does not create any cusps, the constant α could be taken very small ($\alpha = 5\Delta l/20\pi$ was chosen). For the sine flow, a very small $\Delta l = 0.005$ was necessary, for the PDF of scalar to be converged. It might come from the sensitivity to initial conditions of this flow, linked to its well known chaotic behaviour. The constant α also had to be taken very large since the flow creates many cusps. We needed to increase it up to $\alpha = 25\Delta l/\pi$.

(iii) Computational time: The strip diffusion method has been implemented on Matlab, in order to use standard instructions for the resolution of ordinary differential equations, and spline interpolation. This choice made the computation slower than using FORTRAN or C, but that did not matter since the method is extremely fast: the vortex in § 2.6 lasted one hour on a PC at 1.1 GHz and 1.24 Go of RAM. The sine flow computations (with $\Delta l = 0.005$, a number of points per cusps given by $\alpha = 25\Delta l/\pi$ and a time interval $\delta t = 0.001$) took 4 h to calculate the field up to $t = 4$, and a week to extend it to $t = 7$ due to the exponentially large number of tracers generated by the method.

(iv) Computational cost: The strip diffusion method consists in following tracers along a strip advected by a flow. In an exponential flow like the sine flow, the number of tracers defining the strip needs to increase in proportion to the strip length, that is

exponentially fast in time. This might look as a drawback of the method. It is not in fact since in spite of this, it remains competitive with grid-based methods computing the scalar gradients directly: a standard direct numerical simulation of (1.2) will need a number of grid points of the order of

$$N_p = \left(\frac{L}{\sqrt{D/\gamma}}\right)^2 \sim Pe, \tag{A 2}$$

for a domain size L in two dimensions, in order to resolve properly the concentration gradients whose size scales as the Batchelor scale (2.12).

Now the strip diffusion method has already characterized the mixing properties of the flow (spectrum, shape of PDFs, presence or absence of aggregation, etc.) at the mixing time t_s or after a few mixing times. After that, the field is completely mixed and close to uniformity (see e.g. figure 7). The maximal number of tracers needed to keep in memory is thus given by the amount of line stretching at the mixing time

$$N_p = \mathrm{e}^{\gamma t_s} \sim \sqrt{Pe}, \tag{A 3}$$

with t_s given by (2.10) a number which can be substantially smaller than the number of grid points needed for the same Péclet number, when Pe becomes large. This is in addition to the advantage presented by the method that only one computation is needed per flow, the Péclet number being varied at will *a posteriori*, as mentioned in § 2.

REFERENCES

Allègre, C. J. & Turcotte, D. L. 1986 Implications of a two-component marble-cake mantle. *Nature* **323**, 123–127.

Alvarez, M. M., Muzzio, F. J., Cerbelli, S., Adrover, A. & Giona, M. 1998 Self-similar spatiotemporal structure of intermaterial boundaries in chaotic flows. *Phys. Rev. Lett.* **81** (16), 3395–3398.

Arnold, V. I. & Avez, A. 1967 *Problèmes Ergodiques de la Mécanique Classique*. Gauthier-Villars Editeur.

Batchelor, G. K. 1959 Small-scale variation of convected quantities like temperature in a turbulent fluid. Part 1. General discussion and the case of small conductivity. *J. Fluid Mech.* **5**, 113–133.

Beigie, D., Leonard, A. & Wiggins, S. 1991 A global study of enhanced stretching and diffusion in cahotic tangles. *Phys. Fluids* A **3** (5), 1039–1050.

Buch, K. A. Jr., & Dahm, W. J. A. 1996 Experimental study of the fine-scale structure of conserved scalar mixing in turbulent shear flows. Part 1. $Sc \gg 1$. *J. Fluid Mech.* **317**, 21–71.

Cerbelli, S., Alvarez, M. M. & Muzzio, F. J. 2002 Prediction and quantification of micromixing in laminar flows. *AIChE J.* **48** (4), 686–700.

Cerbelli, S., Vitacolonna, V., Adrover, A. & Giona, M. 2004 Eigenvalue-eigenfunction analysis of infinitely fast reactions and micromixing in regular and chaotic bounded flows. *Chem. Engng Sci.* **59**, 2125–2144.

Corrsin, S. 1952 Simple theory of an idealized turbulent mixer. *AIChE J.* **3** (3), 329–330.

Danckwerts, P. V. 1952 The definition and measurement of some characteristics of mixtures. *Appl. Sci. Res.* A **3**, 279.

Dimotakis, P. E. & Catrakis, H. J. 1999 Turbulence, fractals and mixing. In *Mixing Chaos and Turbulence* (ed. H. Chaté, E. Villermaux & J. M. Chomaz). Kluwer Academic/Plenum Publishers.

Duplat, J., Innocenti, C. & Villermaux, E. 2010 A non-sequential turbulent mixing process. *Phys. Fluids* **22**, 035104.

Duplat, J. & Villermaux, E. 2000 Persistency of material element deformation in isotropic flows and growth rate of lines and surfaces. *Eur. Phys. J.* B **18**, 353–361.

Duplat, J. & Villermaux, E. 2008 Mixing by random stirring in confined mixtures. *J. Fluid Mech.* **617**, 51–86.

Falkovich, G., Gawedzki, K. & Vergassola, M. 2001 Particles and fields in fluid turbulence. *Rev. Mod. Phys.* **73** (4), 913–975.

Fannjiang, A., Nonnenmacher, S. & Wolonski, L. 2004 Dissipation time and decay of correlations. *Nonlinearity* **17**, 1481–1508.

Fereday, D. R. & Haynes, P. H. 2004 Scalar decay in two-dimensional chaotic advection and batchelor-regime turbulence. *Phys. Fluids* **16** (12), 4359–4370.

Fountain, G. O., Khakhar, D. V. & Ottino, J. M. 1998 Visualization of three-dimensional chaos. *Science* **281**, 683–686.

Fox, R. O. 2004 *Computational Models for Turbulent Reacting Flows*. Cambridge University Press.

Gardiner, C. W. 2003 *Handbook of Stochastic Methods*. Springer.

Graham, R. & Schenzle, A. 1982 Carleman imbedding of multiplicative stochastic processes. *Phys. Rev.* A **25** (3), 1731–1754.

Jones, S. V. 1994 Interaction of chaotic advection and diffusion. *Chaos Solitons Fractals* **4** (6), 929–940.

Kalda, J. 2000 Simple model of intermittent passive scalar turbulence. *Phys. Rev. Lett.* **84** (3), 471–474.

Kraichnan, R. H. 1974 Convection of a passive scalar by a quasi-uniform random straining field. *J. Fluid Mech.* **64**, 737–732.

Leonard, A. 2009 Overview of turbulent and laminar diffusion and mixing. In *Analysis and Control of Mixing with an Application to Micro and Macro Flow Processes* (ed. L. Cortelezzi & I. Mezic). CISM courses and lectures, vol. 510, Springer.

Levèque, M. A. 1928 Les lois de la transmission de la chaleur par convection. *Ann. Mines* **13**, 201–239.

Marble, F. E. 1988 Mixing, diffusion and chemical reaction of liquids in a vortex field. In *Chemical Reactivity in Liquids: Fundamental Aspects* (ed. M. Moreau & P. Turq), pp. 581–596. Plenum Press.

Marble, F. E. & Broadwell, J. E. 1977 The coherent flame model for turbulent chemical reactions. *Tech. Rep.* TRW-9-PU. Project SQUID.

Meunier, P. & Villermaux, E. 2003 How vortices mix. *J. Fluid Mech.* **476**, 213–222.

Meunier, P. & Villermaux, E. 2007 Van Hove singularities in probability density functions of scalars. *C.R. Méc.* **335**, 162–167.

Moffatt, H. K. 1983 Transport effects associated with turbulence with particular attention to the influence of helicity. *Rep. Prog. Phys.* **46**, 621–664.

Mohr, W. D., Saxton, R. L. & Jepson, C. H. 1957 Mixing in laminar-flow systems. *Indust. Engng Technol.* **49** (11), 1855–1856.

Monin, A. S. & Yaglom, A. M. 1975 *Statistical Fluid Mechanics: Mechanics of Turbulence,* Vol. 2, The MIT Press.

Ottino, J. M. 1989 *The Kinematics of Mixing: Stretching, Chaos, and Transport*. Cambridge University Press.

Perugini, D., Ventura, G., Petrelli, M. & Poli, G. 2004 Kinematic significance of morphological structures generated by mixing of magmas: a case study from salina island (southern Italy). *Earth Planet. Sci. Lett.* **222**, 1051–1066.

Peters, N. 1984 Laminar diffusion flamelet models in non-premixed turbulent combustion. *Prog. Energy Combust. Sci.* **10** (3), 319–339.

Phelps, J. H. & Tucker, C. 2006 Lagrangian particle calculations of distributive mixing: limitations and applications. *Chem. Engng Sci.* **61**, 6826–6836.

Ranz, W. E. 1979 Application of a stretch model to mixing, diffusion and reaction in laminar and turbulent flows. *AIChE J.* **25** (1), 41–47.

Rhines, P. B. & Young, W. R. 1983 How rapidly is a passive scalar mixed within closed streamlines. *J. Fluid Mech.* **133**, 133–145.

Richardson, L. F. 1922 *Weather Prediction by Numerical Process*. Cambridge University Press.

Richardson, L. F. 1926 Atmospheric diffusion shown on a distance-neighbour graph. *Proc. R. Soc. Lond.* A **110**, 709–737.

Robinson, M., Cleary, P. & Monaghan, J. 2008 Analysis of mixing in a twin cam mixer using smoothed particle hydrodynamics. *AIChE J.* **54** (8), 1987–1998.

Shankar, P. N. & Kidambi, R. 2009 Mixing in internally stirred flows. *Proc. R. Soc. Lond.* A **465**, 1271–1290.

Sturman, R., Ottino, J. M. & Wiggins, S. 2006 *The Mathematical Foundations of Mixing*. Cambridge University Press.

Sukhatme, J. & Pierrehumbert, R. T. 2002 Decay of passive scalars under the action of single scale smooth velocity fields in bounded two-dimensional domains: from non-self-similar probability distribution functions to self-similar eigenmodes. *Phys. Rev.* E **66**, 056302.

Thiffeault, J. L., Doering, C. R. & Gibbon, J. D. 2004 A bound on mixing efficiency for the advection diffusion equation. *J. Fluid Mech.* **521**, 105–114.

Toussaint, V., Carrière, P., Scott, J. & Gence, J. N. 2000 Spectral decay of a passive scalar in chaotic mixing. *Phys. Fluids* **12** (11), 2834–2844.

Van Kampen, N. G. 1981 *Stochastic Processes in Chemistry and Physics*. North-Holland Publishing Company.

Villermaux, E. & Duplat, J. 2003 Mixing as an aggregation process. *Phys. Rev. Lett.* **91** (18), 184501.

Villermaux, E. & Duplat, J. 2006 Coarse grained scale of turbulent mixtures. *Phys. Rev. Lett.* **97**, 144506.

Villermaux, E. & Gagne, Y. 1994 Line dispersion in homogeneous turbulence: stretching, fractal dimensions and micromixing. *Phys. Rev. Lett.* **73** (2), 252–255.

Villermaux, E. & Rehab, H. 2000 Mixing in coaxial jets. *J. Fluid Mech.* **425**, 161–185.

Villermaux, E., Stroock, A. D. & Stone, H. A. 2008 Bridging kinematics and concentration content in a chaotic micromixer. *Phys. Rev.* E **77** (1, Part 2).

Welander, P. 1955 Studies on the general development of motion in a two-dimensional, ideal fluid. *Tellus* **7** (2), 141–156.

Yeung, P. K. 2002 Lagrangian investigations of turbulence. *Annu. Rev. Fluid Mech.* **34**, 115–142.

Yeung, P. K., Xu, S. & Sreenivasan, K. R. 2002 Schmidt number effects on turbulent transport with uniform mean scalar gradient. *Phys. Fluids* **14** (12), 4178–4191.

Zabusky, N. J., Hughes, M. H. & Roberts, K. V. 1979 Contour dynamics for the euler equations in 2 dimensions. *J. Comp. Phys.* **30** (1), 96–106.

Zeldovich, Y. B. 1982 Exact solution of the diffusion problem in a periodic velocity field and turbulent diffusion. *Dokl. Akad. Nauk SSSR* **226** (4), 821–826.